

Compound chondrule formation in optically thin shock waves

SOTA ARAKAWA¹ AND TAISHI NAKAMOTO¹

¹*Department of Earth and Planetary Sciences, Tokyo Institute of Technology, Meguro, Tokyo 152-8551, Japan*

ABSTRACT

Shock-wave heating within the solar nebula is one of the leading candidates for the source of chondrule-forming events. Here, we examine the possibility of compound chondrule formation via optically thin shock waves. Several features of compound chondrules indicate that compound chondrules are formed via the collisions of supercooled precursors. We evaluate whether compound chondrules can be formed via the collision of supercooled chondrule precursors in the framework of the shock-wave heating model by using semi-analytical methods and discuss whether most of the crystallized chondrules can avoid destruction upon collision in the post-shock region. We find that chondrule precursors immediately turn into supercooled droplets when the shock waves are optically thin and they can maintain supercooling until the condensation of evaporated fine dust grains. Owing to the large viscosity of supercooled melts, supercooled chondrule precursors can survive high-speed collisions on the order of 1 km s^{-1} when the temperature is below $\sim 1400 \text{ K}$. From the perspective of the survivability of crystallized chondrules, shock waves with a spatial scale of $\sim 10^4 \text{ km}$ may be potent candidates for the chondrule formation mechanism. Based on our results from one-dimensional calculations, a fraction of compound chondrules can be reproduced when the chondrule-to-gas mass ratio in the pre-shock region is $\sim 2 \times 10^{-3}$, which is approximately half of the solar metallicity.

Keywords: hydrodynamics — shock waves — meteorites, meteors, meteoroids — protoplanetary disks

1. INTRODUCTION

Chondrules are millimeter-sized spherical igneous grains contained within chondrites, which are the most common type of meteorites, as a major component. The volume fraction of chondrules in ordinary chondrites is 60–80% (e.g., Rubin 2000; Scott 2007), and the ages of chondrules are approximately 4.563–4.567 billion years, i.e., they were formed during the first 4 million years of the solar system (e.g., Connelly et al. 2012; Bollard et al. 2017). Therefore, they must contain a wealth of information regarding the evolution of the solar nebula. In the canonical view, small dust grains in the solar nebula grew into millimeter-sized aggregates, after which chondrules were formed by the melting of these aggregates in the early solar nebula and became spherical owing to their surface tension (e.g., Zanda 2004); however, their precise origin is still unclear.

Some chondrules, referred to as compound chondrules, are composed of two or more chondrules fused together. They comprise a low percentage of all chondrules (e.g., 4% in ordinary chondrites; Gooding & Keil 1981); however, they may offer crucial information regarding the physical state of solid materials during chondrule formation because they occur not only in ordinary chondrites but also in many classes of chondrites (e.g., Akaki & Nakamura 2005; Bischoff et al. 2017).

Although the formation process of compound chondrules is still under debate, we can interpret the presence of compound chondrules as the result of collisions (e.g., Gooding & Keil 1981; Ciesla et al. 2004b; Miura et al. 2008b; Bogdan et al. 2019). The ubiquitous existence of cratered chondrules (approximately 10% of all chondrules) also indicates that some of the chondrules have experienced collision when they crystallize (e.g., Gooding & Keil 1981). Wasson et al. (1995) examined compound chondrules in thin sections and classified each constituent chondrule as primary or secondary. Primary chondrules retain their spherical shape, while secondary chondrules are deformed. Compound chondrules with blurred intrachondrule boundaries are extremely rare within ordinary chondrites (Wasson et al. 1995). Therefore, most compound chondrules are formed by collisions between crystallized chondrules and non-crystallized precursors (Arakawa & Nakamoto 2016a), or at least two components with a significant viscosity difference to be able to distinguish primary and secondary chondrules (Yasuda et al. 2009).

Chondrules exhibit various textures, reflecting their different compositions and thermal histories (e.g., Gooding & Keil 1981). In general, the textures of chondrules are classified into three textural types, that is, porphyritic, nonporphyritic, and glassy. Porphyritic chondrules consist of phenocrysts of olivine and/or low-calcium pyroxene, with accessory amounts of sulfides and metal nuggets suspended in mesostasis. Nonporphyritic chondrules are usually classi-

fied into three subtypes (e.g., Gooding & Keil 1981): cryptocrystalline, composed of nanometer- and micrometer-sized fine grains; radial-pyroxene; and barred-olivine chondrules (barred-pyroxene and radial-olivine chondrules also exist but are minor components). Glassy chondrules are extremely rare, and they are only mentioned occasionally (e.g., Krot & Rubin 1994). It is typically thought that nonporphyritic and glassy chondrules are formed from completely molten precursors, while porphyritic chondrules melt incompletely during their formation (e.g., Lofgren & Russell 1986; Hewins & Radomsky 1990), although porphyritic textures can also be reproduced from completely molten precursors (e.g., Connolly & Hewins 1995; Srivastava et al. 2010).

Here, we note that the textures of chondrules contained in compound chondrules have noteworthy features. Gooding & Keil (1981) and Wasson et al. (1995) reported that approximately 15% of all chondrules in ordinary chondrites are nonporphyritic, and most of them have porphyritic textures. In contrast, when we observe the components in compound chondrules, most of the constituent chondrules are nonporphyritic (Wasson 1993; Wasson et al. 1995). For the case of compound chondrules in ordinary chondrites, Wasson et al. (1995) revealed that 81% of primaries and 90% of secondaries are nonporphyritic chondrules, and the same trend is also reported by Akaki & Nakamura (2005) for compound chondrules in CV carbonaceous chondrites. Therefore, compound chondrules selectively form from precursors of nonporphyritic chondrules. Dynamic crystallization experiments (e.g., Tsukamoto et al. 1999; Nagashima et al. 2006, 2008) have revealed that completely molten levitated precursors having no contact turn into supercooled droplets as they are cooled sufficiently below their liquidus temperature. In addition, once these supercooled droplets collide with other particles, they crystallize instantaneously (e.g., Connolly et al. 1994). Therefore, when a crystallized chondrule and a supercooled precursor collide and stick together, a compound chondrule is formed (Arakawa & Nakamoto 2016a). This supercooled-collision scenario is consistent with the observed feature of the textures of chondrules contained in compound chondrules because the precursors of nonporphyritic chondrules selectively turn into supercooled droplets.

Numerous ideas have been proposed as mechanisms for single-chondrule formation, including shock-wave heating (e.g., Hood & Horányi 1991; Iida et al. 2001; Boley et al. 2013; Mai et al. 2018), planetesimal collisions (e.g., Asphaug et al. 2011; Dullemond et al. 2014; Johnson et al. 2015; Wakita et al. 2017), and radiative heating by lightning (e.g., Horányi et al. 1995; Desch & Cuzzi 2000; Muranushi 2010; Johansen & Okuzumi 2018). The combination of theoretical calculations and observations of chondrules provides several constraints on the properties of the chondrule formation mechanisms. For example, the shapes of chondrules are usually close to perfect spheres, but some of them have prolate shapes (Tsuchiyama et al. 2003); these prolate shapes can be explained by the rotation of molten chondrules exposed to a fast gas flow in the framework of the shock-

wave heating model (Miura et al. 2008a). The maximum and minimum sizes of chondrules are also consistent with the theoretical predictions of shock-wave heating models (e.g., Susa & Nakamoto 2002; Miura & Nakamoto 2005).

Shock-wave heating within the solar nebula is one of the leading candidates for the source of chondrule-forming transient events. Shock waves could be created by the eccentric planetesimals/protoplanets perturbed by Jovian resonances and the secular resonance caused by the gravity of the protoplanetary disk (e.g., Weidenschilling et al. 1998; Nagasawa et al. 2019) or by gravitational instabilities in the protoplanetary disk (e.g., Boss & Durisen 2005; Boley & Durisen 2008). The process of heating chondrule precursors by shock waves has been investigated in detail in many previous studies. The shock-wave heating model can satisfy various first-order constraints related to chondrule formation, such as the peak temperature and the formation age (e.g., Desch et al. 2012).

One important challenge for shock-wave heating models was noted by Nakamoto & Miura (2004) and Jacquet & Thompson (2014): chondrule precursors of different sizes have different velocities in the post-shock region, and they should collide at a high speed (approximately a few km s^{-1}), which may cause their destruction rather than compound chondrule formation upon collision. However, the critical velocity for collisional sticking/destruction may strongly depend on the physical states of colliding precursors, e.g., phase, temperature, and size ratio. For example, Ciesla (2006) argued that partially molten chondrules with highly viscous outer layers could survive high-speed collisions because energy dissipation in droplet collisions increases as the viscosity of the liquid is increased (e.g., Ennis et al. 1991; Willis & Orme 2003). We note that the viscosity of silicate melts strongly depends on the temperature, and supercooled droplets must have significantly high viscosity (e.g., Fulcher 1925); therefore, the collision of supercooled chondrule precursors in post-shock regions can potentially explain the formation of compound chondrules. In addition, for the case of optically thin shock waves, collisions of chondrule precursors mostly occur when they are in the supercooled state.

In this study, we examine the possibility of compound chondrule formation via optically thin shock waves. We evaluate whether compound chondrules can be formed via the collision of supercooled chondrule precursors in the framework of the shock-wave heating model by using semi-analytical methods and discuss whether most of the crystallized chondrules can avoid destruction upon collision in the post-shock region. The objectives of this study are to postulate how the supercooling of chondrule precursors could affect the outcomes of high-speed collisions and suggest a novel scenario for compound chondrule formation.

2. MODELS

2.1. Outline

Most of the previous studies on chondrule-forming shock-wave heating models assumed that the shock waves are opti-

cally thick and chondrules are thermally coupled with gas in post-shock regions (e.g., [Morris & Desch 2010](#)); however, optically-thick shock waves have a critical issue in the context of compound chondrule formation. Chondrules in optically thick shock waves should maintain a high temperature above their liquidus in post-shock regions (e.g., [Morris & Desch 2010](#)), and molten chondrules cannot avoid collisional destruction if they are in the molten state (e.g., [Jacquet & Thompson 2014](#)). Therefore, in this study, we examine the scenario whereby compound chondrules are formed via optically thin shock waves. The prominent feature of the optically thin shock-wave model is its rapid cooling as a result of radiative cooling (e.g., [Ciesla et al. 2004a](#)).

The formation process of single and compound chondrules in an optically thin shock wave is illustrated in Figure 1. There are chondrule precursors and fine dust grains in the pre-shock region; the fine dust grains should evaporate immediately after passing the shock front, while the chondrule precursors are converted into molten droplets (e.g., [Miura & Nakamoto 2005](#)). There are no fine dust grains immediately behind the shock front, and these evaporated dust grains recondense when the gas temperature drops below the dust condensation temperature T_c (in this study, we assume $T_c = 1600$ K). Molten precursors formed via the passage of the shock front quickly transform into supercooled droplets because of their radiative cooling, and the temperature of supercooled droplets is controlled by the balance between the energy transfer from hot gas molecules to cold droplets and the radiative cooling of droplets (see Equation 45). Although most of the precursors are in the supercooled state before the recondensation of fine dust grains, some precursors experience collision and become crystallized chondrules before the recondensation of fine dust grains. Moreover, if a crystallized chondrule and a supercooled precursor collide and stick together, a compound chondrule is formed ([Arakawa & Nakamoto 2016a](#)). Finally, the gas temperature decreases and the recondensation of fine dust grains occurs downstream, after which supercooled survivors collide with fine dust grains and turn into crystallized chondrules.

2.2. Chondrule dynamics

In this study, we consider one-dimensional normal shocks, as in previous studies (e.g., [Nakamoto & Miura 2004](#); [Ciesla 2006](#); [Jacquet & Thompson 2014](#)). We do not calculate the thermal/dynamical evolution of gas behind the shock front; we assume a simple gas structure, so that the dynamics of chondrules is simulated in the given gas flow. We assume that the gas velocity with respect to the shock front v_g and the gas density ρ_g change across the shock front as functions of the distance from the shock front x as follows:

$$v_g = \begin{cases} v_0 & (x < 0), \\ v_0 + (v_{\text{post}} - v_0) \exp(-x/L) & (x \geq 0), \end{cases} \quad (1)$$

and

$$\rho_g = \begin{cases} \rho_{g,0} & (x < 0), \\ (v_g/v_0)^{-1} \rho_{g,0} & (x \geq 0), \end{cases} \quad (2)$$

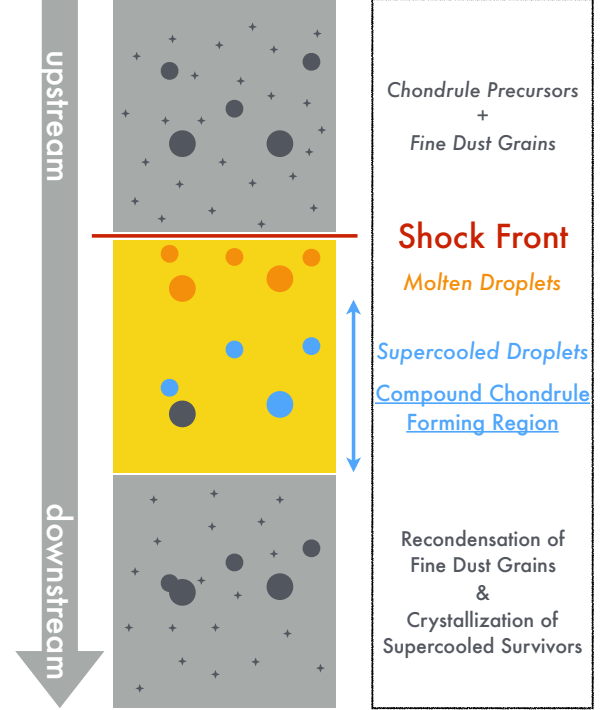


Figure 1. Outline of our compound chondrule formation scenario. Molten chondrule precursors formed via passage of the shock front immediately turn into supercooled droplets because of their radiative cooling. Then, some supercooled precursors experience collision and become crystallized chondrules, and if a crystallized chondrule and a supercooled precursor collide and stick together, a compound chondrule is formed.

where v_0 is the pre-shock gas velocity with respect to the shock front, v_{post} is the post-shock gas velocity with respect to the shock front, $\rho_{g,0}$ is the pre-shock gas density, and L is the spatial scale of the chondrule-forming shock. The post-shock gas velocity, v_{post} , is given by the Rankine–Hugoniot relations as $v_{\text{post}} = [(\gamma - 1)/(\gamma + 1)]v_0$, where γ is the ratio of specific heats. In this study, we set $\rho_{g,0} = 3 \times 10^{-9}$ g cm $^{-3}$, $v_0 = 12$ km s $^{-1}$, and $\gamma = 1.4$. Similarly, the temperature of the gas T_g is assumed as follows:

$$T_g = \begin{cases} T_0 & (x < 0), \\ T_0 + (T_{\text{post}} - T_0) \exp(-x/L) & (x \geq 0), \end{cases} \quad (3)$$

and we assume that the pre-shock gas temperature is $T_0 = 500$ K and the post-shock gas temperature is $T_{\text{post}} = 2000$ K. The sound velocity c_s is given by $c_s \equiv (2k_B T_g / m_g)^{1/2}$, where $k_B = 1.38 \times 10^{-16}$ erg K $^{-1}$ is the Boltzmann constant, and we set the gas molecule mass $m_g = 3.34 \times 10^{-24}$ g, which values correspond to H $_2$ gas.

The velocity of chondrules with respect to the shock front, v , will change as a function of the distance from the shock front x (e.g., [Hood & Horányi 1991](#)):

$$\frac{4\pi}{3} r^3 \rho \frac{dv}{dx} = -\frac{C_D}{2} \pi r^2 \rho_g \frac{|v - v_g|}{v} (v - v_g), \quad (4)$$

where C_D is the drag coefficient, r is the chondrule radius, and $\rho = 3.3 \text{ g cm}^{-3}$ is the internal density of chondrules (Ciesla et al. 2004a). The drag coefficient C_D is given by

$$C_D = \frac{2}{3s} \sqrt{\frac{\pi T}{T_g}} + \frac{2s^2 + 1}{\sqrt{\pi} s^3} \exp(-s^2) + \frac{4s^4 + 4s^2 - 1}{2s^4} \text{erf}(s), \quad (5)$$

where the temperature of the chondrule is T , and s is given by $s \equiv |v - v_g|/c_s$. The drag coefficient C_D is a function of the normalized relative velocity s , and we note that C_D approaches

$$C_D \simeq 2, \quad (6)$$

for the supersonic limit (i.e., $s \gg 1$) and

$$C_D \simeq \frac{16\sqrt{\pi}}{3s} \left(\sqrt{\frac{T}{T_g}} + \frac{1}{8\pi} \right), \quad (7)$$

for the subsonic limit (i.e., $s \ll 1$). We can understand the dynamics of chondrules by considering the stopping length l_{stop} . For the case in which chondrules move in gas with supersonic velocities, l_{stop} is approximately given by

$$l_{\text{stop}} \equiv \left(\frac{1}{v} \frac{dv}{dx} \right)^{-1} \simeq \frac{4}{3} \frac{\rho}{\rho_g} \left(\frac{v - v_g}{v} \right)^{-2} r \sim 2 \times 10^2 \left(\frac{v}{v - v_g} \right)^2 \left(\frac{r}{1 \text{ mm}} \right) \cdot \left(\frac{\rho_g}{2 \times 10^{-8} \text{ g cm}^{-3}} \right)^{-1} \text{ km}. \quad (8)$$

If the spatial scale of shock L is much larger than l_{stop} , the velocity of a chondrule v reaches v_{post} behind the shock front, while v barely changes when $L \ll l_{\text{stop}}$ (see Figure 3b).

The equation of energy for a chondrule in gas is given by (e.g., Hood & Horányi 1991)

$$\frac{4\pi}{3} r^3 \rho c_{\text{heat}} \frac{dT}{dx} = \frac{4\pi r^2}{v} (\Gamma - \Lambda), \quad (9)$$

where $c_{\text{heat}} = 1 \times 10^7 \text{ erg g}^{-1} \text{ K}^{-1}$ is the specific heat (Ciesla et al. 2004a), Γ is the heating rate via gas–chondrule energy transfer per unit area, and Λ is the rate of radiative cooling per unit area. In this study, the effects of latent heat and evaporation (e.g., Miura et al. 2002) are not considered for simplicity. The heating rate via gas–chondrule energy transfer Γ is

$$\Gamma = \rho_g |v - v_g| (T_{\text{rec}} - T) C_H, \quad (10)$$

where T_{rec} is the adiabatic recovery temperature and C_H is the heat transfer function, called the Stanton number. The adiabatic recovery temperature T_{rec} and the Stanton number

C_H are given by (e.g., Gombosi et al. 1986)

$$T_{\text{rec}} = \frac{T_g}{\gamma + 1} \left[2\gamma + 2(\gamma - 1)s^2 - \frac{\gamma - 1}{(1/2) + s^2 + (s/\sqrt{\pi}) \exp(-s^2) \text{erf}^{-1}(s)} \right], \quad (11)$$

and

$$C_H = \frac{\gamma + 1}{\gamma - 1} \frac{k_B}{8m_g s^2} \left[\frac{s}{\sqrt{\pi}} \exp(-s^2) + \left(\frac{1}{2} + s^2 \right) \text{erf}(s) \right]. \quad (12)$$

We assume that the optical depth of the chondrule-forming region is not far larger than unity and chondrules are thermally decoupled from the gas. Here, we check the validity of this assumption. We define \mathcal{R}_w as the width of the warm region (i.e., the region with a gas temperature of $T_g \gg T_0$), and the width of the heating region whose optical depth is unity, $\mathcal{R}_{w,1}$, can be estimated as follows:

$$\mathcal{R}_{w,1} = (\kappa \rho_g)^{-1} \sim 10^3 \left(\frac{\rho_g}{3 \times 10^{-9} \text{ g cm}^{-3}} \right)^{-1} \text{ km}, \quad (13)$$

where $\kappa \sim 3 \text{ cm}^2 \text{ g}^{-1}$ is the opacity of the solar-metallicity protoplanetary disk (e.g., Pollack et al. 1985). Therefore, if the width of the heating region \mathcal{R}_w is not larger than $\mathcal{R}_{w,1}$, and we do not consider significant enrichment of fine dust grains in the solar nebula, we can apply the optically thin approximation for chondrule-forming shock waves. The width of the heating region \mathcal{R}_w is roughly given by the planetary radius \mathcal{R}_p when the shock waves are caused by eccentric planetary bodies (e.g., Boley et al. 2013). Under the optically thin shock assumption, the rate of radiative cooling per unit area of a chondrule Λ is given by

$$\Lambda = \epsilon \sigma_{\text{SB}} T^4 - \epsilon \sigma_{\text{SB}} T_0^4, \quad (14)$$

where $\epsilon = 0.9$ is the Planck mean emission/absorption coefficient (Ciesla et al. 2004a) and $\sigma_{\text{SB}} = 5.67 \times 10^{-5} \text{ erg cm}^{-2} \text{ K}^{-4} \text{ s}^{-1}$ is the Stefan-Boltzmann constant.

2.3. Size-frequency distribution

Several studies (e.g., Rubin & Grossman 1987; Nelson & Rubin 2002; Metzler 2018) have focused on chondrule size-frequency distributions. The size-frequency distributions of chondrules usually use \emptyset -units, which are defined by,

$$\emptyset \equiv -\log_2 \frac{2r}{1 \text{ mm}}, \quad (15)$$

or we can rewrite the above equation as $r = 2^{-(\emptyset+1)} \text{ mm}$. The mass of chondrules $m(\emptyset)$ is given by $m(\emptyset) = (4\pi/3)\rho r^3$.

Here, we assume that the size-frequency distribution in the pre-shock region $f_0(\emptyset)$ is similar to the size-frequency distribution in chondrites (Jacquet 2014); although Kadono & Arakawa (2005) proposed that the size-frequency

distribution may originate from the breakup of huge molten precursors. The size-frequency distribution of chondrules in ordinary chondrites is approximately log-normal (e.g., [Rubin & Grossman 1987](#); [Nelson & Rubin 2002](#)),

$$f_0(\varnothing) \propto \exp \left[-\frac{1}{2} \left(\frac{\varnothing - \varnothing_{\text{mean}}}{\varnothing_{\text{SD}}} \right)^2 \right]; \quad (16)$$

although, in reality, it is known that there is a cutoff for small chondrule sizes (e.g., [Eisenhour 1996](#); [Metzler 2018](#)). In this study, we assume $\varnothing_{\text{mean}} = 0.8$ and $\varnothing_{\text{SD}} = 0.8$, which are the mean and deviation for chondrules in LL ordinary chondrites ([Nelson & Rubin 2002](#)). The total number density of chondrules in pre-shock region N_0 is given by

$$N_0 = \frac{\rho_{c,0}}{\int_{\varnothing_{\text{min}}}^{\varnothing_{\text{max}}} d\varnothing f_0(\varnothing)m(\varnothing)}, \quad (17)$$

where $\rho_{c,0}$ is the mass density of chondrules in the pre-shock region, and \varnothing_{min} and \varnothing_{max} are the minimum and maximum of \varnothing in the size-frequency distribution, respectively (in this study, we set $\varnothing_{\text{min}} = -3$ and $\varnothing_{\text{max}} = +3$). The size-frequency distribution in the pre-shock region satisfies $\int_{\varnothing_{\text{min}}}^{\varnothing_{\text{max}}} d\varnothing f_0 = 1$ by definition. The number density of chondrules whose size is \varnothing , $n_0(\varnothing)$, is also given by

$$n_0(\varnothing) = f_0(\varnothing)N_0. \quad (18)$$

The number density of chondrules in the post-shock region, $n(\varnothing, x)$, changes with changing chondrule velocity $v = v(\varnothing, x)$. Under the one-dimensional normal shock approximation, $n(\varnothing, x)$ is given as follows:

$$n(\varnothing, x) = n_0(\varnothing) \frac{v_0}{v(\varnothing, x)}. \quad (19)$$

Using the geometrical optics approximation, the mean opacity of chondrules, κ_c , is given by

$$\kappa_c = \frac{\int_{\varnothing_{\text{min}}}^{\varnothing_{\text{max}}} d\varnothing n(\varnothing, x) \pi r^2}{\int_{\varnothing_{\text{min}}}^{\varnothing_{\text{max}}} d\varnothing n(\varnothing, x) m}, \quad (20)$$

and κ_c in the pre-shock region is $\kappa_{c,0} = 3.67 \text{ cm}^2 \text{ g}^{-1}$. We found that κ_c is dominated by 0.5 mm-sized chondrules in the pre-shock region. When we take into account the contribution of κ_c , the optical depth of the heating region, τ , is evaluated from

$$\tau = (\kappa \rho_g + \kappa_c \rho_c) \mathcal{R}_w, \quad (21)$$

the latter term, $\kappa_c \rho_c$, is negligibly smaller than the former term, $\kappa \rho_g$, however.

2.4. Collision frequency

Here, we describe how to calculate the collision frequency of chondrules. We define $\zeta_{t,p}$ as the collision frequency per unit distance of a target chondrule, whose size is \varnothing_t , with a

projectile chondrule, whose size is \varnothing_p . Then, $\zeta_{t,p}$ is given as follows:

$$\zeta_{t,p}(\varnothing_t, \varnothing_p, x) = n(\varnothing_p, x) \cdot \pi (r_t + r_p)^2 \cdot \frac{|v(\varnothing_p, x) - v(\varnothing_t, x)|}{v(\varnothing_t, x)}. \quad (22)$$

The collision frequency of a target chondrule with any projectile, Z_t , is therefore given by

$$Z_t(\varnothing_t, x) = \int_{\varnothing_{\text{min}}}^{\varnothing_{\text{max}}} d\varnothing_p \zeta_{t,p}(\varnothing_t, \varnothing_p, x). \quad (23)$$

Finally, the expected number of collisions for each target chondrule after passing the shock front, Σ_t , is given by

$$\Sigma_t(\varnothing_t, x) = \int_0^x dx' Z_t(\varnothing_t, x'). \quad (24)$$

Here, we note that the fraction of compound chondrules among all the nonporphyritic chondrules in ordinary chondrites is approximately 20% ([Ciesla et al. 2004b](#); [Arakawa & Nakamoto 2016a](#)). Therefore, the expected number of collisions Σ_t should be on the order of 20% for small chondrules whose radii are comparable to that of typical secondaries, and Σ_t may be ~ 1 – 2 for large chondrules whose radii are comparable to that of typical primaries because primaries have experienced collisions twice (see Section 2.1 and [Arakawa & Nakamoto 2016a](#)).

2.5. Critical velocity for collisional sticking/merging

When a droplet collides with a solid sphere, the expected collision outcomes are sticking, bouncing, or splashing (e.g., [Josserand & Thoroddsen 2016](#)). Similarly, when two droplets collide, the collision outcomes are merging, bouncing/separation, or splashing (e.g., [Qian & Law 1997](#)). Bouncing usually occurs for grazing collisions. In this study, we examine the critical velocity for compound chondrule formation from the view point of whether supercooled droplets can stick or not. For the description of droplet collisions, it is necessary to consider the physical properties involved: viscosity η , density ρ , and surface tension σ , as well as geometrical properties of the system such as droplet radius r and the impact velocity v_{imp} .

2.5.1. Dimensionless parameters for describing droplet collisions

Using dimensional analysis, we can easily identify the relevant dimensionless parameters to describe binary collisions of liquid droplets (e.g., [Ashgriz & Poo 1990](#)). For the case of head-on collision of equal-sized droplets with identical liquids, the basic parameters are the Weber number We , the Reynolds number Re , and the capillary number Ca :

$$We \equiv \frac{2\rho r v_{\text{imp}}^2}{\sigma}, \quad (25)$$

$$Re \equiv \frac{2\rho r v_{\text{imp}}}{\eta}, \quad (26)$$

$$\text{Ca} \equiv \frac{\eta v_{\text{imp}}}{\sigma} \equiv \frac{\text{We}}{\text{Re}}. \quad (27)$$

For the inviscid fluid limit (i.e., $\text{Ca} \ll 1$), the criteria for collisional sticking should be given by the critical value of the Weber number $\text{We}_{\text{cr},i}$;

$$\text{We} < \text{We}_{\text{cr},i}, \quad (28)$$

and, for the viscous fluid limit (i.e., $\text{Ca} \gg 1$), the criteria should be given by the critical value of the Reynolds number $\text{Re}_{\text{cr},v}$;

$$\text{Re} < \text{Re}_{\text{cr},v}. \quad (29)$$

This expression can be converted into the expression of the critical Weber number by using the capillary number as follows:

$$\text{We} < \text{Re}_{\text{cr},v} \text{Ca}. \quad (30)$$

Therefore, we can imagine that the critical Weber number for collisional sticking, We_{cr} , can be given by the following equation:

$$\text{We}_{\text{cr}} \simeq \text{Re}_{\text{cr},v} \text{Ca} + \text{We}_{\text{cr},i}. \quad (31)$$

2.5.2. Criteria proposed by Sommerfeld & Kuschel (2016)

Droplets are affected by large deformation and energy dissipation when they collide; therefore, it is logical to use Ca , which is the ratio of viscous forces to surface tension forces, for the expression of We_{cr} . Recently, Sommerfeld & Kuschel (2016) proposed an equation for We_{cr} as follows:

$$\text{We}_{\text{cr}} = \frac{K^3}{3} \text{Ca} + 2K, \quad (32)$$

where $K = 6.9451$ is called the structure parameter (Naue & Bärwolff 1992), and we obtain $\text{We}_{\text{cr}} = 111.66\text{Ca} + 13.89$ (see Appendix A).

From Equation (32), we can calculate the critical velocity for head-on collision of equal-sized droplets v_{cr} as follows:

$$v_{\text{cr}}(\eta, r) = \frac{K^3}{12} \frac{\eta}{\rho r} \left(1 + \sqrt{1 + \frac{144}{K^5} \frac{\rho \sigma r}{\eta^2}} \right), \quad (33)$$

and when v_{cr} are controlled by viscous dissipation, these critical velocities are given by $v_{\text{cr}} \sim 55.8\eta/(\rho r)$. In this case, the critical velocities are proportional to the viscosity and inversely proportional to the droplet radius.

For the case of collisions of different-sized droplets with different viscosities, the critical velocity for collisional merging v_{merge} is not yet understood (Li et al. 2016). In this study, we evaluate v_{merge} from the geometric mean of v_{cr} of the target and projectile:

$$v_{\text{merge}} = \sqrt{v_{\text{cr}}(\eta_t, r_t) \cdot v_{\text{cr}}(\eta_p, r_p)}, \quad (34)$$

where η_t and η_p are the viscosities of the target and projectile, respectively. Likewise, when a non-crystallized projectile collides with a solidified target chondrule, we evaluate

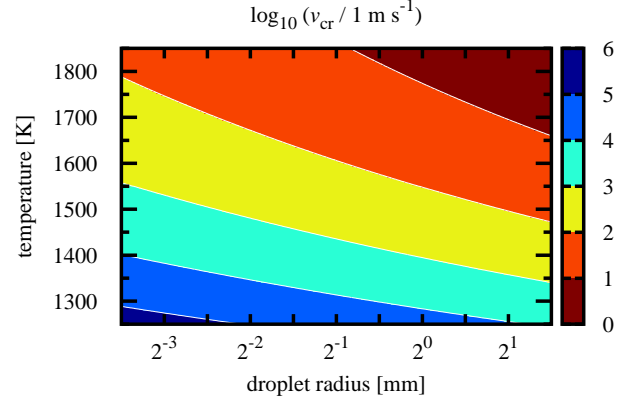


Figure 2. The critical velocity v_{cr} as a function of the radius of colliding droplets r and their temperature T . The viscosity of chondrule droplets is obtained from Equation (36).

the critical velocity for collisional sticking v_{stick} from v_{cr} of the projectile (see Appendix B):

$$v_{\text{stick}} = v_{\text{cr}}(\eta_p, r_p). \quad (35)$$

The colliding supercooled droplets can turn into compound chondrules when the impact velocity v_{imp} is lower than v_{stick} . We note that our evaluation of v_{merge} and v_{stick} is not more than a rough order-of-magnitude estimate, and future studies on this issue are needed.

To determine the critical velocity for collisional sticking/merging, we need to know the material properties of silicate melts, η and σ . Hubbard (2015) calculated the viscosities of chondrule melts by using the formula of Giordano et al. (2008) which is based on the Vogel–Fulcher–Tammann viscosity equation (Vogel 1921; Fulcher 1925; Tammann & Hesse 1926);

$$\log_{10} \frac{\eta}{1 \text{ P}} = -3.55 + \frac{5084.9 \text{ K}}{T - 584.9 \text{ K}}. \quad (36)$$

In contrast, the surface energy is only slightly dependent on the temperature, and we set $\sigma = 400 \text{ erg cm}^{-2}$ (Murase & McBirney 1973).

The calculated v_{cr} is shown in Figure 2. There is a strong dependence of v_{cr} on T , and we found that supercooled chondrule precursors could survive high-speed collisions on the order of 1 km s^{-1} when the temperature is below 1400 K .

2.5.3. Temperature increase after collision

When a droplet collides and sticks with another chondrule, the kinetic energy of the droplet is converted into thermal energy. The impact energy E_{imp} and the thermal energy E_{th} are given by

$$E_{\text{imp}} = \frac{1}{2} \frac{m_t m_p}{m_t + m_p} v_{\text{imp}}^2, \quad (37)$$

and

$$E_{\text{th}} = m_p \rho c_{\text{heat}} \Delta T, \quad (38)$$

where m_t and m_p are the masses of the target and the projectile, respectively. By assuming $E_{\text{th}} \simeq E_{\text{imp}}$, the increase in the droplet temperature ΔT is estimated as follows:

$$\Delta T \sim 1.5 \times 10^2 \left(1 + \frac{m_p}{m_t}\right)^{-1} \left(\frac{v_{\text{imp}}}{1 \text{ km s}^{-1}}\right)^2 \text{ K}. \quad (39)$$

This order estimation implies that, when the impact velocity v_{imp} is far larger than a few km s^{-1} and the projectile-to-target mass ratio m_p/m_t is lower than unity, the colliding supercooled droplet would evaporate after collision rather than turn into a compound chondrule because the increase in the droplet temperature would be $\Delta T \gtrsim 1000 \text{ K}$ (although we should consider the effect of the latent heat in reality). Conversely, the effect of ΔT is negligible when $v_{\text{imp}} \ll 1 \text{ km s}^{-1}$ or $m_p/m_t \gg 1$. Hence we do not consider an increase in temperature after collision for simplicity.

2.6. Catastrophic disruption criteria

It is known that fragments of chondrules are common in chondrites (Nelson & Rubin 2002), and fragmentation could have occurred in the solar nebula; for example, chondrule fragments within enveloping compound chondrules are fragmented in the solar nebula (Wasson et al. 1995). After the crystallization of chondrule precursors, the disruption of chondrules could occur in the post-shock region via high-speed collisions. The catastrophic disruption criteria is $E_{\text{imp}} \leq (m_t + m_p)Q_{\text{RD}}^*$, and the critical specific energy for catastrophic disruption Q_{RD}^* is given by (Stewart & Leinhardt 2009)

$$Q_{\text{RD}}^* = q_s \left(\frac{r_{\text{C1}}}{1 \text{ cm}}\right)^{9\mu/(3-2\varphi)} \left(\frac{v_{\text{imp}}}{1 \text{ cm s}^{-1}}\right)^{2-3\mu} \text{ erg g}^{-1}, \quad (40)$$

where q_s , μ , and φ are dimensionless material properties, and the normalized radius r_{C1} is given as follows:

$$r_{\text{C1}} = \left(\frac{3}{4\pi} \frac{m_t + m_p}{1 \text{ g cm}^{-3}}\right)^{1/3}. \quad (41)$$

For intact rocks such as basalt and granite, Stewart & Leinhardt (2009) reported that the dimensionless material properties of $q_s = 7 \times 10^4$, $\mu = 0.5$, and $\varphi = 8$ provide a reasonable fit for the experimental data. Therefore the critical velocity for catastrophic disruption, v_{disrupt} , is given as follows:

$$v_{\text{disrupt}} = 5.12 \times 10^3 \left(\frac{m_t}{m_p}\right)^{2/3} \left(1 + \frac{m_p}{m_t}\right)^{49/39} \cdot \left(\frac{m_t}{10^{-3} \text{ g}}\right)^{-1/13} \text{ cm s}^{-1}. \quad (42)$$

Collisional disruption experiments with chondrules in Allende CV3 chondrite have been performed by Ueda et al. (2001), and they revealed that the catastrophic disruption criteria for similar-sized chondrules is approximately $1.5 \times 10^4 \text{ cm s}^{-1}$. This experimental result validates our evaluation of v_{disrupt} .

3. RESULTS

3.1. Chondrule dynamics and thermal history

We first show the chondrule dynamics and thermal history in optically thin shock waves. Here, we consider small and large shock waves whose spatial scales are $L = 100 \text{ km}$ and $L = 10000 \text{ km}$, respectively. Figure 3 shows the velocity of chondrules with respect to the shock front v and gas velocity v_g . Figure 3a clearly shows that v does not approach $v_{\text{post}} (= 2 \text{ km s}^{-1})$ for the small-scale shock wave. In contrast, for the large-scale shock wave (Figure 3b), v approaches v_{post} in the post-shock region. This is because the stopping length of chondrules l_{stop} is significantly smaller than the spatial scale L (see Equation 8). For the case of Figure 3b, both v and v_g change simultaneously when the distance from the shock front x is larger than 1000 km . We derive an analytical equation of the chondrule-to-gas relative velocity, $v - v_g$, in Section 3.5.

Figure 4 is the temperature of chondrules T and the gas temperature T_g . The gray vertical line represents the recondensation line of evaporated fine dust grains (i.e., the location where the gas temperature is $T_g = T_c$). In this study, we set the condensation temperature to $T_c = 1600 \text{ K}$.

The liquidus temperature of chondrules is in the range of $1600\text{--}2100 \text{ K}$ (e.g., Cohen et al. 2000), and the solidus temperature is approximately 1400 K (e.g., Sanders & Scott 2012), although these temperatures depend on the composition of chondrules and the ambient pressure. When the peak temperature of a chondrule is higher than the solidus temperature but lower than the liquidus temperature, the chondrule turns into a partially molten droplet. In contrast, when the peak temperature is higher than the liquidus temperature, the chondrule becomes a completely molten droplet. For the case of small-scale shock waves (Figure 4a), most of the small chondrules with radii of $r < 0.25 \text{ mm}$ turn into completely molten precursors, while almost all large chondrules with radii of $r > 0.5 \text{ mm}$ become partially molten droplets.

Several experimental studies have revealed that completely molten precursors turn into supercooled droplets and finally become glassy chondrules unless they collide with other particles (e.g., Nagashima et al. 2008). However, the observations of chondrules in a thin section revealed that glassy chondrules are extremely rare (e.g., Krot & Rubin 1994). This fact indicates that the recondensation of evaporated fine dust grains must occur before the temperature of supercooled precursors drops below the glass transition temperature T_{glass} . The glass transition temperature is dependent on the chemical composition, but it may be approximately $T_{\text{glass}} \sim 900\text{--}1000 \text{ K}$ (e.g., Villeneuve et al. 2015). Figure 4a shows that the recondensation of evaporated fine dust grains occurs before the temperature of supercooled precursors drops below the glass transition point; therefore, they can turn into crystallized chondrules without a glass transition.

The heating/cooling history of chondrules in the large-scale shock wave is shown in Figure 4b. As in Figure 4a, recondensation of evaporated fine dust grains occurs before the

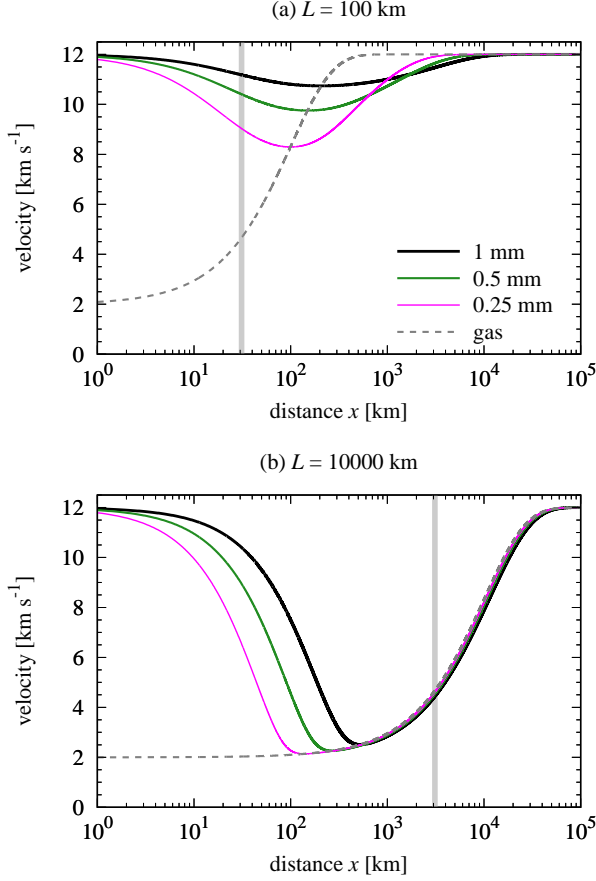


Figure 3. The velocity of chondrules with respect to the shock front v and the gas velocity v_g . (a) For the case of the small-scale shock wave ($L = 100$ km). (b) For the case of the large-scale shock wave ($L = 10000$ km). The solid curves represent the velocity of chondrules with radii of $r = 1$ mm (black), $r = 0.5$ mm (green), and $r = 0.25$ mm (magenta), and the gray dashed curve is the gas velocity. The gray vertical line represents the recondensation line of evaporated fine dust grains.

temperature of supercooled precursors drops below the glass transition temperature, and these supercooled precursors can avoid turning into glassy chondrules. The peak temperature of chondrules only slightly depends on their radii for the case of large-scale shock waves, and they can maintain the supercooling state for a long time.

3.2. Equilibrium temperature of chondrules

After the chondrule-to-gas relative velocity reaches zero (i.e., $s \rightarrow 0$), the temperature of chondrules in high-temperature gas can be calculated from the balance of the heating via collisions of high-temperature gas molecules and the radiative cooling of chondrules. The heating term is given by

$$\Gamma = \frac{1}{8\sqrt{\pi}} \frac{\gamma+1}{\gamma-1} \rho_g c_s^3 \left(1 - \frac{T}{T_g}\right) \equiv \Gamma_g \left(1 - \frac{T}{T_g}\right), \quad (43)$$

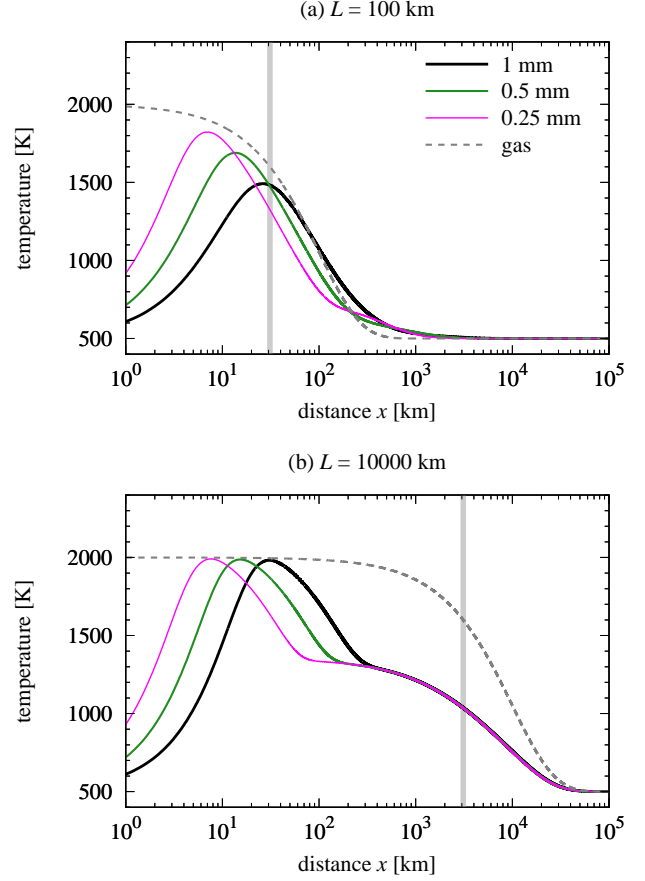


Figure 4. The temperature of chondrules T and the gas temperature T_g . (a) For the case of the small-scale shock wave ($L = 100$ km). (b) For the case of the large-scale shock wave ($L = 10000$ km). The solid curves represent the temperature of chondrules with radii of $r = 1$ mm (black), $r = 0.5$ mm (green), and $r = 0.25$ mm (magenta), and the gray dashed curve is the gas temperature. The gray vertical line represents the recondensation line of evaporated fine dust grains.

and the cooling term is

$$\Lambda = \epsilon \sigma_{\text{SB}} (T^4 - T_0^4) = \Lambda_g \left[\left(\frac{T}{T_g}\right)^4 - \left(\frac{T_0}{T_g}\right)^4 \right], \quad (44)$$

where $\Lambda_g \equiv \epsilon \sigma_{\text{SB}} T_g^4$. Then, we obtain the equilibrium value of T by solving the equation, $\Gamma - \Lambda = 0$, and we can rewrite this equation as follows:

$$\frac{(T/T_g)^4 - (T_0/T_g)^4}{1 - T/T_g} = \frac{\Gamma_g}{\Lambda_g}. \quad (45)$$

We find that there are two limiting cases; one case is that $T/T_g \rightarrow 1$ and $\Gamma_g/\Lambda_g \rightarrow \infty$, and the other case is that $T/T_g \rightarrow T_0/T_g$ and $\Gamma_g/\Lambda_g \rightarrow 0$. The dimensionless parameter Γ_g/Λ_g is given by

$$\frac{\Gamma_g}{\Lambda_g} = 0.696 \left(\frac{\rho_g}{2 \times 10^{-8} \text{ g cm}^{-3}} \right) \left(\frac{T_g}{2000 \text{ K}} \right)^{-5/2}. \quad (46)$$

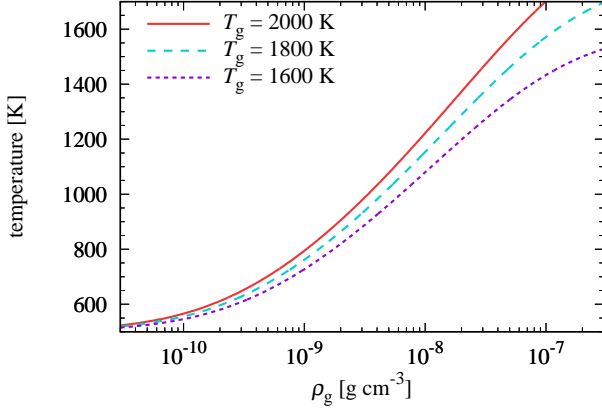


Figure 5. The temperature of chondrule precursors T as a function of the gas density and the gas temperature, ρ_g and T_g , under the assumption of $v - v_g = 0$. The temperature of chondrule precursors is calculated from Equation (45) and we set $T_0 = 500$ K.

Then, we can calculate the equilibrium temperature of chondrules in high-temperature gas as a function of the gas density and the gas temperature, ρ_g and T_g . Figure 5 shows that completely molten droplets turn into supercooled droplets with a temperature of $900 \text{ K} < T < 1400 \text{ K}$ when the gas density in the post-shock region is on the order of $\rho_g \sim 10^{-8} \text{ g cm}^{-3}$, where $T_{\text{glass}} \simeq 900 \text{ K}$ is the glass transition temperature and $T \lesssim 1400 \text{ K}$ is the condition for surviving high-speed collisions (Section 2.5.2). Therefore, the preferred value of the gas density in the pre-shock region, $\rho_{g,0}$, is on the order of 10^{-9} – $10^{-8} \text{ g cm}^{-3}$ because the gas density increases after the passage of the shock front. We note, however, that the lower limit of ρ_g to maintain the supercooling of chondrule precursors is also dependent on the background temperature (in this study, we simply assume that the background temperature is the same as the pre-shock gas temperature, $T_0 = 500 \text{ K}$). In addition, the effective background temperature may be affected by the optical depth of the chondrule-forming region when the optical depth is close to unity. We will study the three-dimensional (or axisymmetric two-dimensional) radiative hydrodynamics of planetary bow shocks in the future.

3.3. Collision frequency

In Section 3.1, we calculated the velocity evolution of chondrules in the post-shock region. The velocity depends on the radius of chondrules, and collision of chondrules occurs towing to the difference in the velocity. Then, we can calculate the collision frequency of chondrules.

Figure 6 shows the collision frequency of a target chondrule with any projectiles, Z_t , and Figure 7 shows the expected number of collisions for each target chondrule after passing the shock front, Σ_t . Here, we assumed that the chondrule mass density in the pre-shock region is $\rho_{c,0} = 6 \times 10^{-12} \text{ g cm}^{-3}$. The chondrule-to-gas mass ratio in the pre-shock region is therefore $\rho_{c,0}/\rho_{g,0} = 2 \times 10^{-3}$, and this

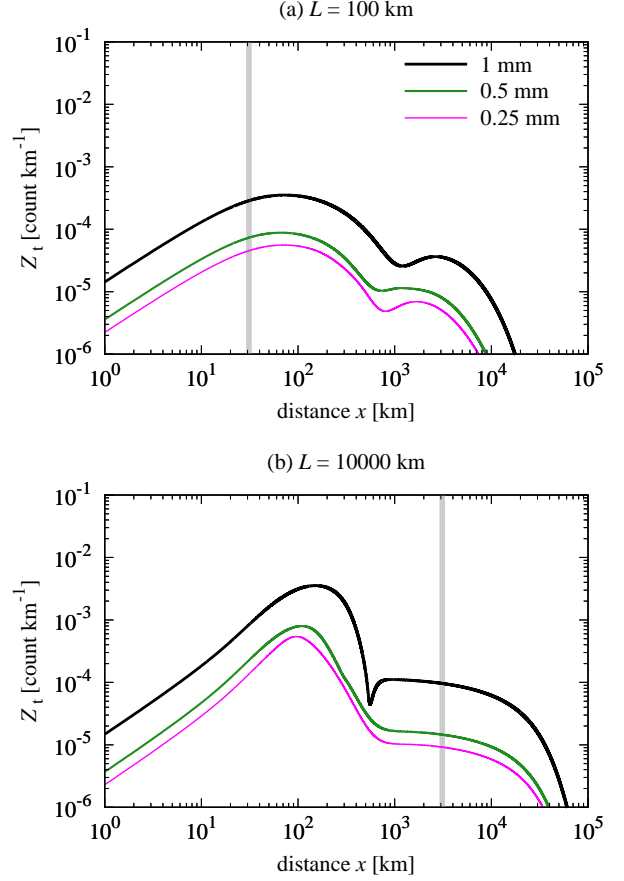


Figure 6. The collision frequency of a target chondrule with any projectile, Z_t . (a) For the case of the small-scale shock wave ($L = 100 \text{ km}$). (b) For the case of the large-scale shock wave ($L = 10000 \text{ km}$). The solid curves represent Z_t of chondrules with radii of $r = 1 \text{ mm}$ (black), $r = 0.5 \text{ mm}$ (green), and $r = 0.25 \text{ mm}$ (magenta). The gray vertical line represents the recondensation line of evaporated fine dust grains. We assumed that the chondrule mass density in the pre-shock region is $\rho_{c,0} = 6 \times 10^{-12} \text{ g cm}^{-3}$.

value is approximately half of the well-assumed silicate-to-gas mass ratio ($= 4.3 \times 10^{-3}$; Miyake & Nakagawa 1993). We can imagine that part of the silicate dust may exist as fine dust grains and others exist as chondrules and/or large dust aggregates. Therefore, our estimate of $\rho_{c,0}/\rho_{g,0} = 2 \times 10^{-3}$ is reasonable to some extent.

As shown in Figures 6 and 7, the collision of chondrules occurs in two stages; the first stage corresponds to where the velocity of chondrules approaches the gas velocity and larger chondrules have larger values of v , and the second stage corresponds to where the velocity of chondrules recover to the pre-shock velocity and smaller chondrules have larger values of v . The frequency of collision depends on the spatial scale L if L is comparable to or smaller than the stopping length of chondrules, i.e., $L \lesssim l_{\text{stop}}$. This fact has been previously mentioned by Jacquet & Thompson (2014), and Z_t

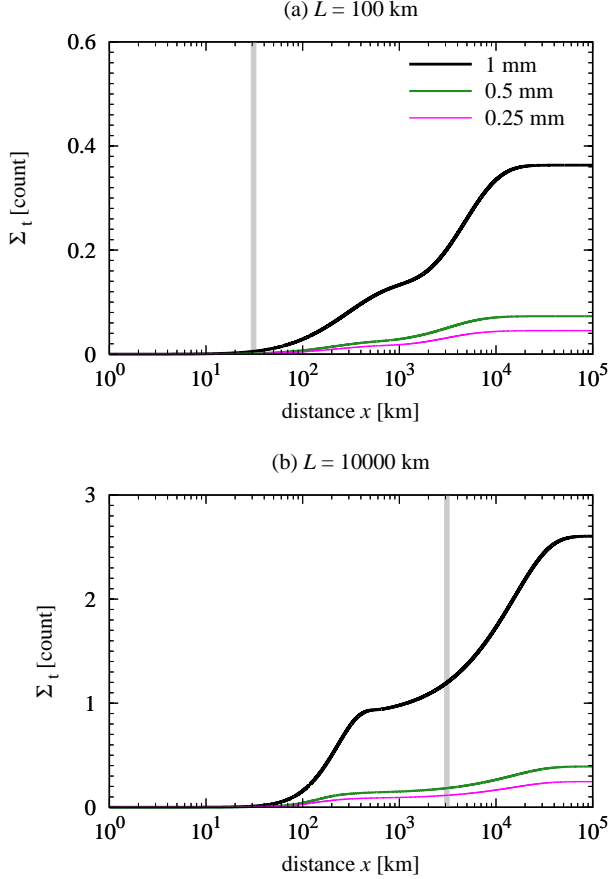


Figure 7. The expected number of collisions for each target chondrule after passing the shock front, Σ_t . (a) For the case of the small-scale shock wave ($L = 100$ km). (b) For the case of the large-scale shock wave ($L = 10000$ km). The solid curves represent Σ_t of chondrules with radii of $r = 1$ mm (black), $r = 0.5$ mm (green), and $r = 0.25$ mm (magenta). The gray vertical line represents the recondensation line of evaporated fine dust grains.

and Σ_t are small for small-scale shock waves compared with the case of large-scale shock waves.

The expected number of collisions for submillimeter-sized chondrules is lower than unity when we assume $\rho_{c,0}/\rho_{g,0} = 2 \times 10^{-3}$; therefore, most of the chondrule precursors that are heated above their liquidus temperature turn into supercooled droplets and can keep their supercooling state until the recondensation of fine dust grains occurs (see Figure 7). Conversely, millimeter-sized large chondrules collide frequently, and for the case of large-scale shock waves, most of the millimeter-sized chondrules experience collision when $\rho_{c,0}/\rho_{g,0} \gtrsim 2 \times 10^{-3}$. After a collision, the supercooled droplet turns into a crystallized chondrule when the collision velocity is below v_{merge} , and some of these chondrules have experienced multiple collisions; this is the mechanism of compound chondrule formation (see Figure 2 of Arakawa & Nakamoto 2016a). We note that the number of collisions Σ_t is proportional to $\rho_{c,0}/\rho_{g,0}$; then, Σ_t

for submillimeter-sized chondrules could also exceed unity when $\rho_{c,0}/\rho_{g,0} \gtrsim 10^{-2}$.

Figure 8 shows the collision frequency of a target chondrule whose size is $r_t = 0.25$ mm with projectile chondrules whose size is r_p . The peak of the collision frequency distribution is located between $r_p = 0.5$ mm and 1 mm for the whole region. This is due to the balance of the impact velocity, the collisional cross section, and the number density of chondrules; large chondrules have large velocities and large cross sections but small number densities. As shown in Figure 7, large chondrules tend to crystallize earlier, and small ones tend to be secondaries. In addition, the peak of the size-frequency distribution is located around $r \sim 0.25$ mm. Therefore, the radius of secondaries r_{sec} may be distributed around $r_{\text{sec}} \sim 0.25$ mm, and the typical radius of primaries r_{pri} may be $r_{\text{pri}} \sim 0.5$ –1 mm.

The secondary-to-primary size ratio, $\Delta_{\text{sp}} \equiv r_{\text{sec}}/r_{\text{pri}}$, has been measured in thin sections by a few studies (e.g., Wasson et al. 1995), and the mean value of Δ_{sp} for compound chondrules in ordinary chondrites is ~ 0.3 . This value seems to be consistent with the calculated collision frequency distribution shown in Figure 8 (see also Figure 9); although the observation in the thin section is somewhat biased and the real value of Δ_{sp} may be somewhat larger than 0.3 (see Ciesla et al. 2004b).

3.4. Collisions of supercooled droplets

In our calculation, we obtain the temperature and the velocity of chondrules simultaneously. Therefore, we can compare the impact velocity of chondrules with different radius v_{imp} and the critical velocity for collisional merging v_{merge} and sticking v_{stick} , which are dependent on the temperature of chondrules. Hereafter, we focus on the case of the large-scale shock wave ($L = 10000$ km).

Figure 9 shows the critical velocity for collisional merging v_{merge} , sticking v_{stick} , and the impact velocity v_{imp} for target chondrules with $r_t = 1$ mm. From Figure 4a, the temperature of chondrules with $r_t = 1$ mm rapidly decreases before the distance from the shock front reaches $x \simeq 300$ km. The critical velocities v_{merge} and v_{stick} are strongly dependent on the temperature of the target and projectile chondrules (see Figure 2). Therefore, both v_{merge} and v_{stick} significantly increase before the distance from the shock front reaches $x \simeq 300$ km. In addition, the impact velocity v_{imp} falls below 1 km s^{-1} for $x \gtrsim 200$ –300 km; then, v_{merge} and v_{stick} overcome v_{imp} .

As a conclusion, compound chondrules with a primary radius of ~ 1 mm would be formed via collisions of supercooled droplets in the post-shock region where the distance from the shock front exceeds $x \gtrsim 300$ km, although the suitable location for compound chondrule formation must depend on the detailed characteristics of the specific chondrule-forming shock waves.

The lower panels of Figure 9 show the $\zeta_{t,p}(\varnothing_t, \varnothing_p, x)$ of supercooled chondrules with a target radius of $r_t = 1$ mm, i.e., $\varnothing_t = -1$. The size-frequency distribution of projectiles is a maximum at $r_p \sim 0.25$ –0.5 mm. As shown in

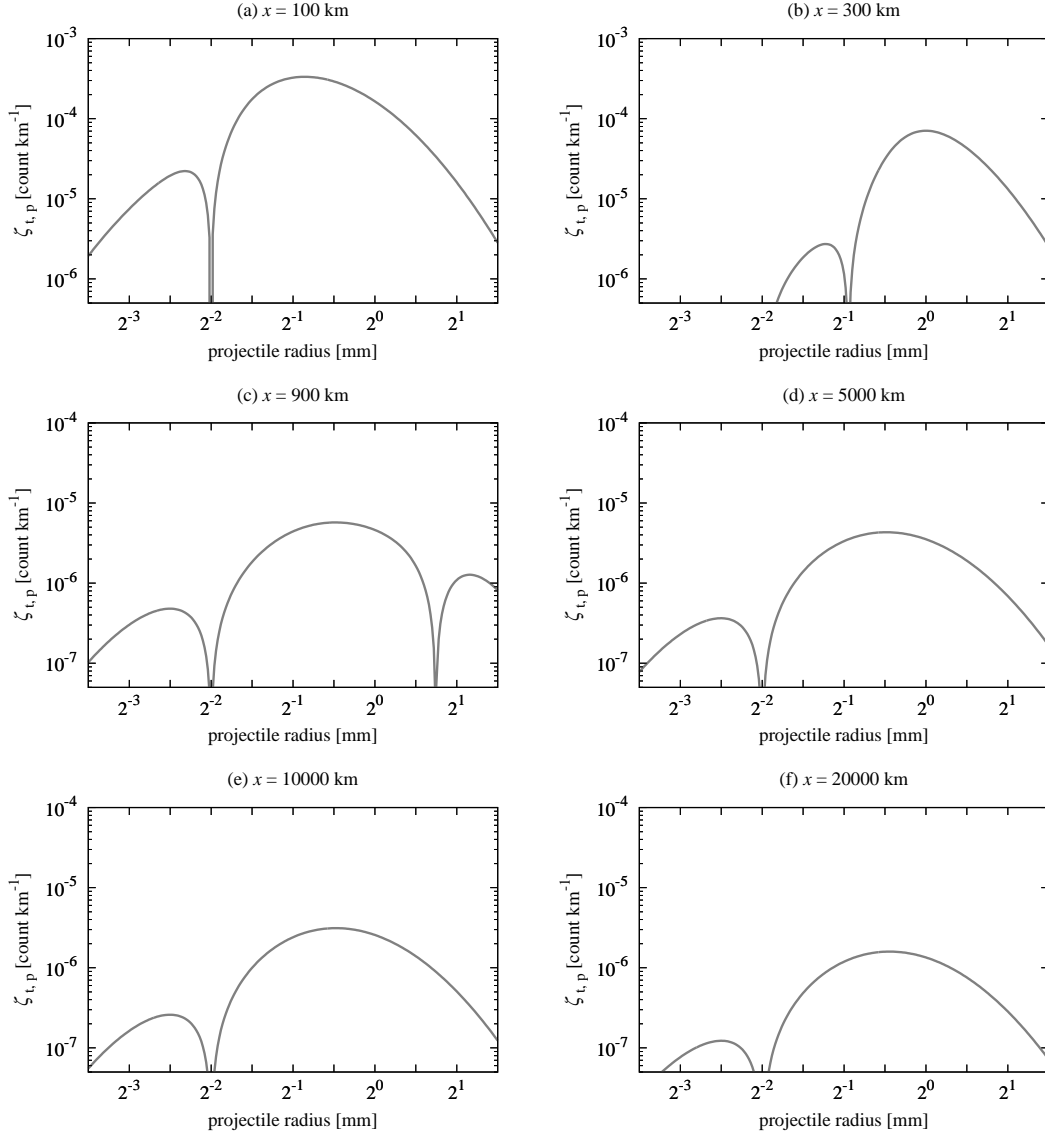


Figure 8. The collision frequency of a target chondrule whose size is $r_t = 0.25$ mm with projectile chondrules whose size is r_p at (a) $x = 100$ km, (b) $x = 300$ km, (c) $x = 900$ km, (d) $x = 5000$ km, (e) $x = 10000$ km, and (f) $x = 20000$ km, respectively. The presented results are for the case of the large-scale shock wave ($L = 10000$ km).

Figure 7, the expected number of collisions Σ_t is lower for smaller chondrules. Then, the probability that the small projectile chondrule is supercooled while the large target chondrule is already crystallized is higher than the probability that the small projectile chondrule is crystallized while the large target chondrule is still in the supercooled state. Therefore, compound chondrules whose secondary-to-primary size ratio is $\Delta_{sp} \sim 0.3$ may be formed via a collision between crystallized and supercooled chondrules in the post-shock region, as already mentioned (see Figure 8).

Here, we note that some of the collisions must cause the splashing of supercooled droplets when they collide with high speed and/or high temperature, although the fraction of disruption is lower than unity when we assume $\rho_{c,0}/\rho_{g,0} \sim 2 \times 10^{-3}$. [Jacquet & Thompson \(2014\)](#) noted that chondrules

can also be destroyed by continuous erosion through the collisions of fragments produced by other catastrophic collision events. In this study, we do not take into consideration this “sandblasting” effect, however. Whether the collisions of fragments would be critical or not is dependent on the size distribution of fragments, and future studies on this point are needed.

3.5. Survivability of crystallized chondrules

The evaporated fine dust grains would recondense when the gas temperature decreases below the dust condensation temperature T_c (we assumed $T_c = 1600$ K in this study). The location of the dust condensation line x_c is therefore $x_c \sim 0.3L$ when we assume the gas temperature is determined by Equation (3). After the recondensation of fine dust grains,

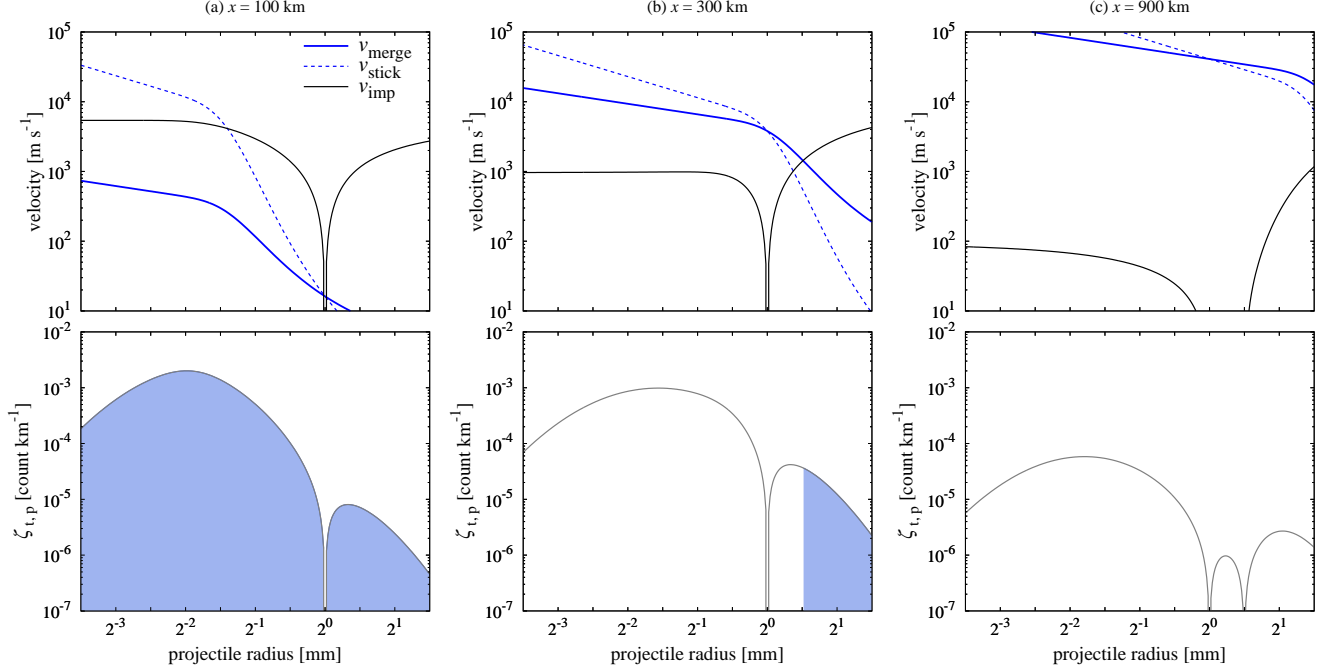


Figure 9. *Upper panels:* the critical velocity for collisional merging v_{merge} , sticking v_{stick} , and the impact velocity v_{imp} . *Lower panels:* the collision frequency of a target chondrule whose size is $r_t = 1$ mm with projectile chondrules $\zeta_{t,p}(\varnothing_t = -1, \varnothing_p, x)$. The shaded regions show where non-crystallized targets would disrupt when they collide with projectiles, i.e., $v_{\text{imp}} > v_{\text{merge}}$. The presented results are for the case of the large-scale shock wave ($L = 10000$ km). (a) The snapshot at $x = 100$ km. (b) The snapshot at $x = 300$ km. (c) The snapshot at $x = 900$ km.

supercooled droplets are crystallized by the accretion of condensates onto chondrule precursors (e.g., Nagashima et al. 2006, 2008).

Here, we investigate whether crystallized chondrules can avoid catastrophic disruption after their crystallization. We compare v_{imp} and v_{disrupt} ; then, the survivability of crystallized chondrules is evaluated. The upper panels of Figure 10 show the critical velocity for catastrophic disruption v_{disrupt} and the impact velocity v_{imp} for target chondrules with $r_t = 1$ mm, and the lower panels show the $\zeta_{t,p}(\varnothing_t, \varnothing_p, x)$ of supercooled chondrules with a target radius of $r_t = 1$ mm.

Without performing numerical simulations, we can roughly evaluate the impact velocity of chondrules by simple analytical calculations. The impact velocity of large and small chondrules is approximately given by the relative velocity of the large chondrule from the gas. The velocity of chondrules with respect to the shock front is given by the following time differential equation:

$$\frac{dv}{dt} = -\frac{3 C_D}{4} \frac{\rho_g}{2 \rho} \frac{|v - v_g|(v - v_g)}{r} \simeq -3c_s \frac{\rho_g}{\rho} \frac{(v - v_g)}{r}, \quad (47)$$

where t is the time and we assume $C_D \sim 8/s$. For the case of large-scale shock waves, the relative velocity of the chondrule from the gas is significantly smaller than the gas velocity, i.e., $|v - v_g| \ll v_g$. Then, the differential of $|v - v_g|$ is also negligible, i.e., $|d(v - v_g)/dt| \ll |dv_g/dt|$. This means

that the differential of the velocity of chondrules is approximately given by the gas velocity and the spatial scale of the shock wave as follows:

$$\left| \frac{dv}{dt} \right| \simeq \left| \frac{dv_g}{dt} \right| \sim \frac{(v_0 - v_{\text{post}})^2}{L}. \quad (48)$$

Therefore, from the combination of Equations (47) and (48), the relative velocity of the chondrule from the gas can be evaluated as follows:

$$\begin{aligned} |v - v_g| &\simeq \frac{1}{3} \frac{\rho}{\rho_g} \frac{r}{L} \frac{(v_0 - v_{\text{post}})^2}{c_s} \\ &\sim 3 \times 10^2 \left(\frac{\rho_g}{10^{-8} \text{ g cm}^{-3}} \right)^{-1} \left(\frac{L}{10^4 \text{ km}} \right)^{-1} \\ &\quad \cdot \left(\frac{r}{1 \text{ mm}} \right) \text{ m s}^{-1}. \end{aligned} \quad (49)$$

Our numerical simulations also confirmed that the typical impact velocity of chondrules of 1 mm in radius is approximately 300 m s^{-1} , and disruptive collisions are minor among all collisions (see Figure 10) when the spatial scale is $L \gtrsim 10000$ km. The expected fraction for catastrophic disruption is, therefore, lower than unity for chondrules whose radius is less than 1 mm in this case. We note that, when the spatial scale is smaller than 100 km (i.e., $L \ll l_{\text{stop}}$), the expected number of collisions itself is far lower than unity, and neither do we need to consider the catastrophic disruption

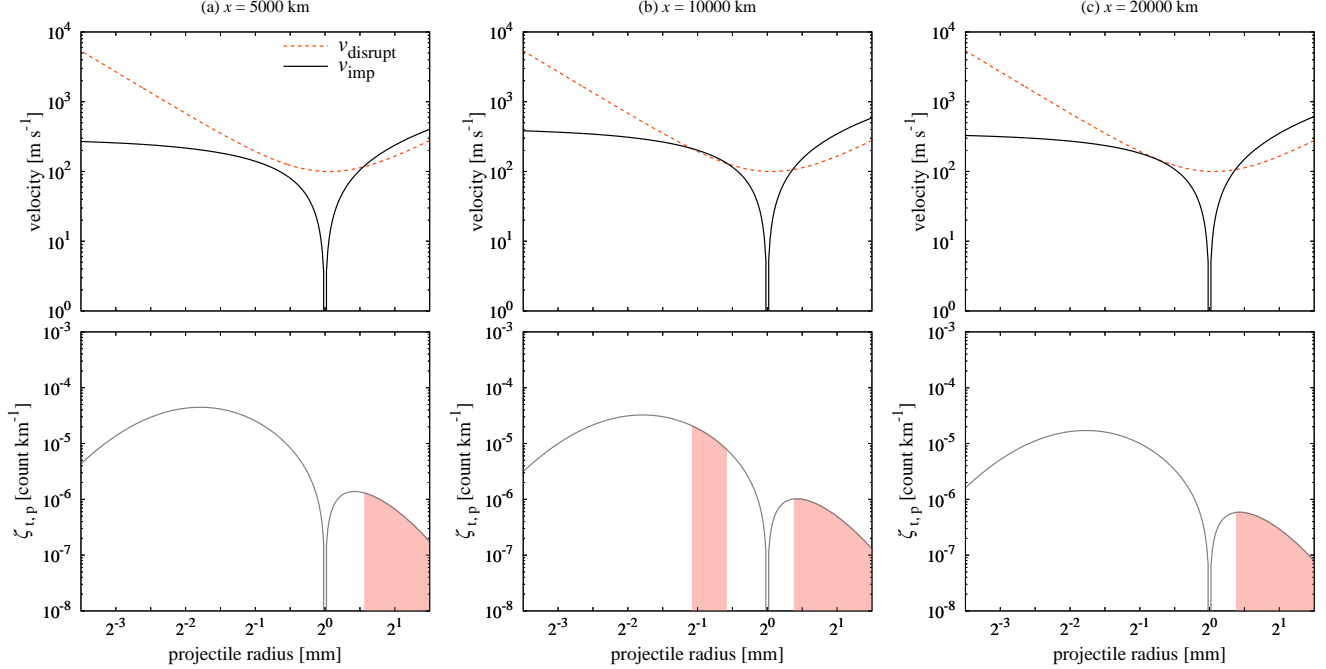


Figure 10. *Upper panels:* the critical velocity for catastrophic disruption v_{disrupt} and the impact velocity v_{imp} . *Lower panels:* the collision frequency of a target chondrule whose size is $r_t = 1$ mm with projectile chondrules $\zeta_{t,p}(\vartheta_t = -1, \vartheta_p, x)$. The shaded regions show where crystallized targets would disrupt when they collide with projectiles, i.e., $v_{\text{imp}} > v_{\text{disrupt}}$. The presented results are for the case of the large-scale shock wave ($L = 10000$ km). (a) The snapshot at $x = 5000$ km. (b) The snapshot at $x = 10000$ km. (c) The snapshot at $x = 20000$ km.

of chondrules, although it depends on the chondrule-to-gas mass ratio.

The impact velocity is inversely proportional to the spatial scale of the shock L , and the necessary condition for chondrule survival may be $L \gtrsim 10000$ km. When the shock waves are caused by eccentric planetary bodies, the spatial scale of the shock wave L is approximately a few to ten times larger than the planetary radius \mathcal{R}_p (e.g., [Morris et al. 2012](#); [Boley et al. 2013](#)), although L/\mathcal{R}_p depends on the opacity, the shock velocity, and so on. Therefore, planetary bow shocks caused by 1000 km-sized protoplanets may be potent candidates for the chondrule formation mechanism from the point of view of chondrule survivability.

4. DISCUSSION

4.1. Chondrule-to-gas mass ratio

It is usually assumed that the silicate-to-gas mass ratio is approximately 4.3×10^{-3} ([Miyake & Nakagawa 1993](#)), and part of the silicate dust can exist as fine dust grains, while others formed chondrules and/or much larger dust aggregates. Therefore, we assume that the chondrule-to-gas mass ratio in the pre-shock region is 2×10^{-3} . However, when chondrules sediment at the midplane of the solar nebula, the chondrule-to-gas mass ratio at the midplane ρ_c/ρ_g becomes significantly higher than the chondrule-to-gas surface density ratio χ . Here, we evaluate whether the sedimentation of chondrules would occur.

When the radius of a chondrule is smaller than the mean-free path of gas molecules, i.e., the gas drag force on the chondrule is determined by Epstein's law, the dimensionless stopping time called the Stokes number St is given by

$$St = \sqrt{\frac{\pi}{8}} \frac{\rho r \Omega_K}{\rho_g c_s} \sim 7 \times 10^{-5} \left(\frac{r}{1 \text{ mm}} \right) \left(\frac{\rho_g}{3 \times 10^{-9} \text{ g cm}^{-3}} \right)^{-1} \cdot \left(\frac{T_0}{500 \text{ K}} \right)^{-1/2} \left(\frac{R}{1 \text{ au}} \right)^{-3/2}, \quad (50)$$

where Ω_K is the Kepler frequency and R is the distance from the sun ([Weidenschilling 1977](#)). The gas scale height h_g is given by $h_g = c_s/\Omega_K$, and the chondrule scale height h_c is given by ([Youdin & Lithwick 2007](#)):

$$\frac{h_c}{h_g} = \left(1 + \frac{St}{\alpha_t} \frac{1 + 2St}{1 + St} \right)^{-1/2}, \quad (51)$$

where α_t is a dimensionless turbulent parameter. Then, the chondrule-to-gas mass ratio at the midplane is given by $\rho_c/\rho_g = (h_c/h_g)^{-1} \chi$.

The value of the dimensionless parameter α_t for our solar nebula is unclear; however, some protoplanetary disks (e.g., the disk around HL Tau) have a turbulent viscosity that is equivalent to α_t in the range of 10^{-4} to 10^{-3}

(e.g., [Pinte et al. 2016](#); [Okuzumi et al. 2016](#)) in the outer regions. Conversely, the dimensionless parameter α_t for the inner region of the disk has not yet been revealed by astronomical observations. Theoretical studies suggest that α_t is up to 10^{-3} or higher when the magneto-rotational instability is active, while α_t may be on the order of 10^{-4} if the magneto-rotational instability is inactive (e.g., [Balbus & Hawley 1991](#)). Therefore, the scale heights of gas and chondrules, h_g and h_c , should be almost the same when the gas density at the midplane is $\rho_g \sim 3 \times 10^{-9} \text{ g cm}^{-3}$. In this case, ρ_c/ρ_g is approximately given by $\rho_c/\rho_g \simeq \chi$ and we do not need to consider the enrichment of chondrules at the disk midplane.

4.2. Location of the chondrule-forming region

We give a constraint on the location of the chondrule formation from the point of view of the gravitational stability of the solar nebula. The stability of the disk is measured by Toomre's Q value, defined by ([Toomre 1964](#)),

$$Q = \frac{c_s \Omega_K}{\pi G \cdot (\sqrt{2\pi} h_g \rho_g)} \simeq 25 \left(\frac{R}{1 \text{ au}} \right)^{-3} \left(\frac{\rho_g}{3 \times 10^{-9} \text{ g cm}^{-3}} \right), \quad (52)$$

and the gas disk becomes unstable when $Q \lesssim 2$ and the above equation gives the upper limit of the gas density.

As shown in [Figure 5](#), the favored gas density to keep molten chondrules in the supercooled state is $\rho_g \sim 10^{-8} \text{ g cm}^{-3}$ in the post-shock region. This value corresponds to $\rho_{g,0} \sim 10^{-9} - 10^{-8} \text{ g cm}^{-3}$ in the pre-shock region. Then, the location of the chondrule-forming region may be within a few astronomical units from the sun if chondrules are formed by optically thin shock waves. This region overlaps with the location of the inner part of the asteroid belt, which is mostly dominated by S-type asteroids (e.g., [DeMeo & Carry 2014](#)), and this coincidence may indicate that chondrules in ordinary chondrites are formed via shock-wave heating in the inner solar nebula because S-type asteroids are the parent bodies of ordinary chondrites ([Nakamura et al. 2011](#)), while chondrules in carbonaceous chondrites may be linked to different events and locations.

4.3. Volatile retention

Chondrules contain volatile elements such as sodium, potassium, and sulfur in their interiors. This implies that chondrules are formed by flash-heating/rapid-cooling events (e.g., [Tachibana & Huss 2005](#); [Rubin 2010](#); [Wasson 2012](#)) or the ambient environments where chondrules melted under a high partial pressure of lithophile elements (e.g., [Alexander et al. 2008](#); [Fedkin & Grossman 2013](#)). The latter hypothesis, called ‘‘dust enrichment’’, originates from the assumption that porphyritic chondrules, which are the main type among all chondrules, may be formed with a low cooling rate ($\sim 10^{-3} - 1 \text{ K s}^{-1}$; [Desch et al. 2012](#), and references therein). This assumption originates from the results of classical furnace-based crystallization experiments

(e.g., [Radomsky & Hewins 1990](#)); however, several estimations based on some chondrule features, such as overgrowth thicknesses on relict grains (e.g., [Wasson & Rubin 2003](#)) and rim formation for barred olivine chondrules ([Miura et al. 2010b](#)), give much higher cooling rates ($\sim 200 - 2000 \text{ K s}^{-1}$; [Miura & Yamamoto 2014](#)). Moreover, porphyritic textures may be reproduced by multiple melting processes (e.g., [Rubin 2010](#)) and they can also be formed via supercooled precursors (e.g., [Srivastava et al. 2010](#); [Seto et al. 2017](#)). Therefore, dust enrichment is not necessarily needed for volatile retainment when the heating/cooling rates around their liquidus temperature are high enough.

In addition, chondrules in different chondrite groups have different average sizes (e.g., [Scott 2007](#)), and chondrite groups with large average chondrule sizes (e.g., CV chondrites) tend to have less bulk sodium than groups with small average chondrule sizes ([Wasson & Kallemeyn 1988](#)) and low proportions of nonporphyritic chondrules ([Rubin 2010](#)). These features can be interpreted as a result of multiple flash-melting events (e.g., [Rubin 2010](#)), and the constraint on the cooling rate can be mitigated.

4.4. Metal grains

Recently, [Libourel & Portail \(2018\)](#) found a notable absence of metal grains in barred olivine chondrules. The absence of metal grains in completely molten chondrule precursors was theoretically predicted by [Uesugi et al. \(2005, 2008\)](#). In addition, the unique occurrence of metal grains in the core region of magnesium-rich olivine crystals of porphyritic chondrules suggests that the metal grains act as seeding agents during the crystal growth of the olivine crystals in porphyritic chondrules ([Libourel & Portail 2018](#)), and the difference in the textures of porphyritic or barred olivine chondrules is linked to the presence/absence of iron-nickel metal grains.

After the ejection of metal grains from molten chondrule precursors, metal grains may collide and merge with other metal grains. [Okabayashi et al. \(2019\)](#) measured the abundances of highly siderophile elements on metal grains from type 3 ordinary chondrites and found that larger metal grains have relatively homogeneous abundances of highly siderophile elements that are close to the bulk metal composition. This observed trend is consistent with the idea that some of the metal grains collided and merged with other metal grains ([Okabayashi et al. 2019](#)). For iron and nickel, [Leliwa-Kopystynski et al. \(1984\)](#) performed collision experiments by using 8 mm-sized projectiles. The critical velocity for collisional sticking is $v_{\text{stick}} \sim 500 \text{ m s}^{-1}$ when the temperature is 290 K, and the estimated v_{stick} at 1800 K is approximately 300 m s^{-1} . Therefore, collisional sticking of ejected metal grains could occur in the post-shock region.

4.5. Early formation of Jupiter

If chondrules are formed by bow shocks caused by eccentric planetary bodies, the existence of both Jupiter and the nebular gas in the chondrule-forming era is a necessary condition. Although the onset of chondrule formation

is still debated (e.g., [Kita & Ushikubo 2012](#); [Bollard et al. 2017](#); [Pape et al. 2019](#)), both lead-lead ages and aluminum-magnesium ages show that the onset of chondrule formation is approximately 2 million years after the formation of calcium-aluminum-rich inclusions, or much earlier. Therefore, Jupiter must be formed within 2 million years in the solar nebula. We note that the early formation of proto-Jupiter is also favored in the context of the chemical dichotomy between carbonaceous and non-carbonaceous meteorite groups (e.g., [Kruijer et al. 2017](#)) and the preservation of calcium-aluminum-rich inclusions in the carbonaceous chondrite formation region ([Desch et al. 2018](#)).

4.6. Accretion of chondrules

There are many studies of the accretion process of chondrules, and some of these studies focus on the effect of fine dust grains accreted onto chondrules. It is known that some of the chondrules in ordinary and carbonaceous chondrites are rimmed by fine dust grains ($\sim 15\%$ for chondrules in Allende CV3 chondrite, [Simon et al. 2018](#)). Theoretical studies have also revealed that free-floating chondrules in a protoplanetary disk can obtain porous dust layers (e.g., [Xiang et al. 2019](#)), which help dust-rimmed chondrules stick together when they collide ([Beitz et al. 2012](#); [Gunkelmann et al. 2017](#)).

Evaporation and recondensation by shock-wave heating events change the size-frequency distribution of fine dust grains (e.g., [Miura et al. 2010a](#)). When the cooling rate of evaporated dust is large, the condensates could be nanograins, which would be beneficial for the direct aggregation of silicate dust aggregates ([Arakawa & Nakamoto 2016b](#)). However, when fluffy aggregates constituted by chondrules and fine dust grains collide at large velocities, the chondrules in fluffy matrices may be ejected to the solar nebula again ([Arakawa 2017](#)). Then, the growth of dust-rimmed chondrules may be impeded when they reach a few centimeters in radius.

Meanwhile, these centimeter-sized aggregates have the potential to turn into planetesimals via the streaming instability driven by differences in the motions of the gas and dust particles in the disk ([Carrera et al. 2015](#); [Yang et al. 2017](#)). In addition, the typical radius of planetesimals formed via the streaming instability is $\sim 10^2$ km ([Simon et al. 2016](#)), which is roughly consistent with the estimated radius of the ordinary chondrite parent bodies (e.g., [Henke et al. 2012a,b](#)).

The other idea is that chondrules accrete onto planetesimals that already exist in the gaseous solar nebula (e.g., [Hasegawa et al. 2016](#); [Matsumoto et al. 2017](#)). [Matsumoto et al. \(2017\)](#) calculated the chondrule accretion onto a protoplanet and planetesimals in the oligarchic growth stage (e.g., [Kokubo & Ida 1998](#)) and found that approximately half of the chondrules accrete onto the protoplanet, while the other half accrete onto planetesimals with an accretion timescale of $\sim 10^6$ years. In this case, some of the chondrules should have stayed in the solar nebula for a few million years; this timescale is consistent with the fact that some of the chondrules have experienced multiple melting

events with the time interval of $\sim 10^6$ years (e.g., [Akaki et al. 2007](#)).

Planetary bodies with moderate eccentricities ($e_p \sim 10^{-2}$ – 10^{-1}) accrete chondrule-sized particles more efficiently than planetary bodies in circular orbits; however, the accretion efficiency drops drastically when the eccentricity becomes far larger than 10^{-1} ([Liu & Ormel 2018](#)). Therefore, it may be difficult to grow eccentric planetesimals/protoplanets into terrestrial planets when they have a large eccentricity. The excitation of eccentricity increases the gas drag; then, the eccentricity and semimajor axis are quickly damped around 1 au ([Nagasawa et al. 2014, 2019](#)), although the location is dependent on the physical properties of the disk. The migration of planetesimals may cause the concentration of circular planetesimals around $R \sim 1$ au. This concentration of planetesimals could have the potential to explain why two large terrestrial planets, Venus and Earth, formed at approximately 1 au (e.g., [Hansen 2009](#); [Walsh & Levison 2016](#)).

5. CONCLUSION

We explored the possibility that compound chondrules are formed via the collisions of supercooled precursors in shock waves. The shock-wave heating model is one of the prime candidates to explain the origin of chondrules. However, there is one challenge to this model: chondrule precursors of different sizes must have different velocities in the post-shock region and they should collide with high speed (approximately a few km s^{-1}), which may lead to their destruction upon collision rather than compound chondrule formation if they were completely molten.

As it is, [Arakawa & Nakamoto \(2016a\)](#) revealed that compound chondrules may be formed via collisions of supercooled precursors. Supercooling is the state where liquids do not solidify even below their solidus temperature. Supercooled chondrule precursors have large viscosity, and their critical velocity for collisional sticking is higher than that of completely molten precursors. Therefore, the destruction of chondrules could be avoided when we consider the supercooling of chondrule precursors.

We calculated the velocity and the temperature of chondrule precursors in optically thin shock waves. We found that, in optically thin shock waves, chondrule precursors can maintain their supercooling until the fine dust grains condense and supercooled precursors crystallize via accretion of fine dust grains. As a first step toward more comprehensive modeling, we considered one-dimensional normal shocks and we assumed a simple gas structure; subsequently, the dynamics of chondrules was simulated in the given gas flow.

Our key findings are summarized as follows.

1. Because supercooled chondrule precursors have a large viscosity, the critical velocity for collisional sticking/merging could be as large as 1 km s^{-1} when the temperature of supercooled droplets is below 1400–1500 K (Figure 2).

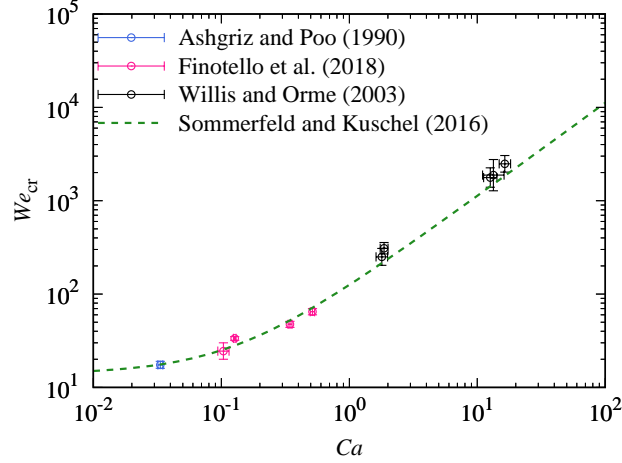


Figure 11. Experimental data of head-on collisions for equal-sized droplets (Ashgriz & Poo 1990; Willis & Orme 2003; Finotello et al. 2018) and the proposed equation of the critical Weber number (Sommerfeld & Kuschel 2016). In these experiments, the Ohnesorge number Oh is given and the range of the critical Weber number We_{cr} is reported. Then, we can evaluate the capillary number Ca from $Ca = Oh\sqrt{We_{cr}}$.

2. Behind the shock front of the shock wave, recondensation of evaporated fine dust grains occurs before the temperature of supercooled precursors drops below the glass transition temperature, and these supercooled precursors can avoid turning into glassy chondrules (Figure 4).
3. The expected number of collisions for submillimeter-sized chondrules is lower than unity when we assume $\rho_{c,0}/\rho_{g,0} = 2 \times 10^{-3}$; therefore, most of the chondrule precursors that are heated above their liquidus temperature turn into supercooled droplets and can maintain their supercooling state until the recondensation of fine dust grains occurs. Conversely, millimeter-sized large chondrules collide frequently, and for the case

of large-scale shock waves with $L \gg l_{stop}$, most of the millimeter-sized chondrules have experienced collision when $\rho_{c,0}/\rho_{g,0} \gtrsim 2 \times 10^{-3}$ (Figure 7).

4. With respect to the survivability of crystallized chondrules, shock waves with a spatial scale of $L \gtrsim 10^4$ km may be desirable because the impact velocity of chondrules is inversely proportional to the spatial scale of the shock wave (Section 3.5).

We thank the anonymous referee for thoughtful comments. This work is supported by JSPS KAKENHI Grant (JP15K05266; JP18K03721). S.A. is supported by the Grant-in-Aid for JSPS Research Fellow (JP17J06861).

APPENDIX

A. DROPLET-DROPLET COLLISION EXPERIMENTS

The dynamics of droplet-droplet collisions has been studied for a long time because of its complexity as a fluid dynamics phenomenon. In particular, understanding the effect of viscosity and surface energy on binary droplet collisions is of great importance for understanding the outcomes of binary equal-sized droplet collision. The dynamics of binary equal-sized droplet collision has been investigated by numerous experimental and numerical studies (e.g., Ashgriz & Poo 1990; Finotello et al. 2017). Sommerfeld & Kuschel (2016) proposed the criteria for collisional sticking as follows:

$$We_{cr} = 111.66Ca + 13.89. \quad (A1)$$

In Figure 11, we checked the validity of the formula given by Sommerfeld & Kuschel (2016) by using the experimental data reported by Ashgriz & Poo (1990), Willis & Orme (2003), and Finotello et al. (2018).

Several previous studies (e.g., Qian & Law 1997; Gotaas et al. 2007) have proposed utilizing the dependence of We_{cr} on the Ohnesorge number Oh . The Ohnesorge number Oh is given by

$$Oh \equiv \frac{\eta}{\sqrt{2\rho\sigma r}} \equiv \frac{Ca}{\sqrt{We}}. \quad (A2)$$

Gotaas et al. (2007) proposed a relationship between We_{cr} and Oh as follows:

$$We_{cr} = \begin{cases} 14.8 + 643.1Oh & (Oh < 0.04), \\ 9309Oh^{1.7056} & (Oh \geq 0.04). \end{cases} \quad (A3)$$

We can rewrite the latter part of Equation (A3) by using Ca instead of Oh :

$$We_{cr} = 138.7Ca^{0.9206}. \quad (A4)$$

The coefficient and the exponent in Equation (A4) are quite close to the coefficient and the exponent in the first term of Equation (A1). In addition, both Equations (A1) and (A3) asymptote to $We_{cr} \simeq 14$ for the inviscid limit ($Ca \rightarrow 0$ and $Oh \rightarrow 0$). These facts support the validity of the criteria for collisional sticking proposed by Sommerfeld & Kuschel (2016).

Recently, Li et al. (2016) investigated the collisions of two droplets with different viscosities, and they revealed that penetration and encapsulation are the typical outcomes for droplet collisions with a high relative viscosity ratio. These collision outcomes may have the potential to form enveloping compound chondrules. Our numerical results also suggest that collision of chondrule precursors frequently occurs with two precursors with different temperature, i.e., different viscosities (see Figure 4).

Compared with equal-size droplet collisions, unequal-size droplet collisions are more relevant to the practical situation of compound chondrule formation. For the case of collision with low-viscosity droplets, Ashgriz & Poo (1990) and Tang et al. (2012) found that the critical impact velocity significantly increases as the size ratio $\Delta \equiv r_{small}/r_{large}$ decreases, where r_{small} and r_{large} are the radii of smaller and larger droplets, respectively. This size-ratio dependence of the critical Weber number may be due to the decrease in the relative kinetic energy determined by the total mass, and a theoretical model that is based on energy balance generally reproduces the experimental trend (Tang et al. 2012). Although we expect that this trend is also shown for collisions between highly viscous droplets, we have no reliable experimental data yet. Future studies on this topic are therefore essential.

B. DROPLET–SOLID COLLISION EXPERIMENTS

The outcome of a droplet impact on a solid surface also depends on the physical properties of the liquid, and there have been several studies on the sticking/splashing criteria of a droplet–solid collision (e.g., Walzel 1980; Mundo et al. 1995; Josserand & Thoroddsen 2016). Considering the equations of energy conservation, Mundo et al. (1995) analytically derived the criteria for collisional sticking/splashing as follows (see also Chandra & Avedisian 1991):

$$We_{cr} = \frac{9}{2}\beta^4 Ca + 3(1 - \cos \Theta)\beta^2 - 12, \quad (B5)$$

where β is the maximum spreading diameter of the droplet scaled with the initial diameter and Θ is the contact angle. Chandra & Avedisian (1991) revealed that the maximum spreading diameter is $\beta \simeq 2-3$, and this relation matches the experimentally obtained correlation between We_{cr} and Ca (Mundo et al. 1995). This equation is a special case of Equation (31), implying that the energy dissipation mechanism in droplet–solid collisions may be similar to that of a droplet–droplet collision. In addition, the equivalent critical Reynolds number is $Re_{cr,v} = (9/2)\beta^4 \sim 10^2$, which is similar to the critical Reynolds number for droplet–droplet collisions.

We acknowledge, however, that the physics of droplet–solid collisions is still not well-understood. Therefore, we roughly evaluate the sticking/splashing criteria of droplet–solid collision by using Equation (35) instead of Equation (B5), and our estimate is no more than an order estimation. We will study droplet–solid collisions by using hydrodynamics simulations in the future.

REFERENCES

- Akaki, T., & Nakamura, T. 2005, *GeoCoA*, 69, 2907, doi: [10.1016/j.gca.2004.12.025](https://doi.org/10.1016/j.gca.2004.12.025)
- Akaki, T., Nakamura, T., Noguchi, T., & Tsuchiyama, A. 2007, *ApJL*, 656, L29, doi: [10.1086/512100](https://doi.org/10.1086/512100)
- Alexander, C. M. O., Grossman, J. N., Ebel, D. S., & Ciesla, F. J. 2008, *Science*, 320, 1617, doi: [10.1126/science.1156561](https://doi.org/10.1126/science.1156561)
- Arakawa, S. 2017, *ApJ*, 846, 118, doi: [10.3847/1538-4357/aa8564](https://doi.org/10.3847/1538-4357/aa8564)
- Arakawa, S., & Nakamoto, T. 2016a, *Icarus*, 276, 102, doi: [10.1016/j.icarus.2016.04.041](https://doi.org/10.1016/j.icarus.2016.04.041)
- . 2016b, *ApJL*, 832, L19, doi: [10.3847/2041-8205/832/2/L19](https://doi.org/10.3847/2041-8205/832/2/L19)
- Ashgriz, N., & Poo, J. Y. 1990, *Journal of Fluid Mechanics*, 221, 183, doi: [10.1017/S0022112090003536](https://doi.org/10.1017/S0022112090003536)
- Asphaug, E., Jutzi, M., & Movshovitz, N. 2011, *Earth and Planetary Science Letters*, 308, 369, doi: [10.1016/j.epsl.2011.06.007](https://doi.org/10.1016/j.epsl.2011.06.007)
- Balbus, S. A., & Hawley, J. F. 1991, *ApJ*, 376, 214, doi: [10.1086/170270](https://doi.org/10.1086/170270)
- Beitz, E., Güttler, C., Weidling, R., & Blum, J. 2012, *Icarus*, 218, 701, doi: [10.1016/j.icarus.2011.11.036](https://doi.org/10.1016/j.icarus.2011.11.036)
- Bischoff, A., Wurm, G., Chaussidon, M., et al. 2017, *Meteoritics and Planetary Science*, 52, 906, doi: [10.1111/maps.12833](https://doi.org/10.1111/maps.12833)
- Bogdan, T., Teiser, J., Fischer, N., Kruss, M., & Wurm, G. 2019, *Icarus*, 319, 133, doi: [10.1016/j.icarus.2018.09.011](https://doi.org/10.1016/j.icarus.2018.09.011)
- Boley, A. C., & Durisen, R. H. 2008, *ApJ*, 685, 1193, doi: [10.1086/591013](https://doi.org/10.1086/591013)

- Boley, A. C., Morris, M. A., & Desch, S. J. 2013, *ApJ*, 776, 101, doi: [10.1088/0004-637X/776/2/101](https://doi.org/10.1088/0004-637X/776/2/101)
- Bollard, J., Connelly, J. N., Whitehouse, M. J., et al. 2017, *Science Advances*, 3, e1700407, doi: [10.1126/sciadv.1700407](https://doi.org/10.1126/sciadv.1700407)
- Boss, A. P., & Durisen, R. H. 2005, *ApJL*, 621, L137, doi: [10.1086/429160](https://doi.org/10.1086/429160)
- Carrera, D., Johansen, A., & Davies, M. B. 2015, *A&A*, 579, A43, doi: [10.1051/0004-6361/201425120](https://doi.org/10.1051/0004-6361/201425120)
- Chandra, S., & Avedisian, C. T. 1991, *Proceedings of the Royal Society of London Series A*, 432, 13, doi: [10.1098/rspa.1991.0002](https://doi.org/10.1098/rspa.1991.0002)
- Ciesla, F. J. 2006, *Meteoritics and Planetary Science*, 41, 1347, doi: [10.1111/j.1945-5100.2006.tb00526.x](https://doi.org/10.1111/j.1945-5100.2006.tb00526.x)
- Ciesla, F. J., Hood, L. L., & Weidenschilling, S. J. 2004a, *Meteoritics and Planetary Science*, 39, 1809, doi: [10.1111/j.1945-5100.2004.tb00077.x](https://doi.org/10.1111/j.1945-5100.2004.tb00077.x)
- Ciesla, F. J., Lauretta, D. S., & Hood, L. L. 2004b, *Meteoritics and Planetary Science*, 39, 531, doi: [10.1111/j.1945-5100.2004.tb00917.x](https://doi.org/10.1111/j.1945-5100.2004.tb00917.x)
- Cohen, B. A., Hewins, R. H., & Yu, Y. 2000, *Nature*, 406, 600, doi: [10.1038/35020514](https://doi.org/10.1038/35020514)
- Connelly, J. N., Bizzarro, M., Krot, A. N., et al. 2012, *Science*, 338, 651, doi: [10.1126/science.1226919](https://doi.org/10.1126/science.1226919)
- Connolly, Jr., H. C., & Hewins, R. H. 1995, *GeoCoA*, 59, 3231, doi: [10.1016/0016-7037\(95\)00207-G](https://doi.org/10.1016/0016-7037(95)00207-G)
- Connolly, Jr., H. C., Hewins, R. H., Atre, N., & Lofgren, G. E. 1994, *Meteoritics*, 29, 458
- DeMeo, F. E., & Carry, B. 2014, *Nature*, 505, 629, doi: [10.1038/nature12908](https://doi.org/10.1038/nature12908)
- Desch, S. J., & Cuzzi, J. N. 2000, *Icarus*, 143, 87, doi: [10.1006/icar.1999.6245](https://doi.org/10.1006/icar.1999.6245)
- Desch, S. J., Kalyaan, A., & Alexander, C. M. O. 2018, *ApJS*, 238, 11, doi: [10.3847/1538-4365/aad95f](https://doi.org/10.3847/1538-4365/aad95f)
- Desch, S. J., Morris, M. A., Connolly, Jr., H. C., & Boss, A. P. 2012, *Meteoritics and Planetary Science*, 47, 1139, doi: [10.1111/j.1945-5100.2012.01357.x](https://doi.org/10.1111/j.1945-5100.2012.01357.x)
- Dullemond, C. P., Stammer, S. M., & Johansen, A. 2014, *ApJ*, 794, 91, doi: [10.1088/0004-637X/794/1/91](https://doi.org/10.1088/0004-637X/794/1/91)
- Eisenhour, D. D. 1996, *Meteoritics and Planetary Science*, 31, 243, doi: [10.1111/j.1945-5100.1996.tb02019.x](https://doi.org/10.1111/j.1945-5100.1996.tb02019.x)
- Ennis, B. J., Tardos, G., & Pfeffer, R. 1991, *Powder Technology*, 65, 257, doi: [10.1016/0032-5910\(91\)80189-p](https://doi.org/10.1016/0032-5910(91)80189-p)
- Fedkin, A. V., & Grossman, L. 2013, *GeoCoA*, 112, 226, doi: [10.1016/j.gca.2013.02.020](https://doi.org/10.1016/j.gca.2013.02.020)
- Finotello, G., Kooiman, R. F., Padding, J. T., et al. 2018, *Experiments in Fluids*, 59, 17, doi: [10.1007/s00348-017-2471-2](https://doi.org/10.1007/s00348-017-2471-2)
- Finotello, G., Padding, J. T., Deen, N. G., et al. 2017, *Physics of Fluids*, 29, 067102, doi: [10.1063/1.4984081](https://doi.org/10.1063/1.4984081)
- Fulcher, G. S. 1925, *Journal of the American Ceramic Society*, 8, 339, doi: [10.1111/j.1151-2916.1925.tb16731.x](https://doi.org/10.1111/j.1151-2916.1925.tb16731.x)
- Giordano, D., Russell, J. K., & Dingwell, D. B. 2008, *Earth and Planetary Science Letters*, 271, 123, doi: [10.1016/j.epsl.2008.03.038](https://doi.org/10.1016/j.epsl.2008.03.038)
- Gombosi, T. I., Nagy, A. F., & Cravens, T. E. 1986, *Reviews of Geophysics*, 24, 667, doi: [10.1029/RG024i003p00667](https://doi.org/10.1029/RG024i003p00667)
- Gooding, J. L., & Keil, K. 1981, *Meteoritics*, 16, 17, doi: [10.1111/j.1945-5100.1981.tb00183.x](https://doi.org/10.1111/j.1945-5100.1981.tb00183.x)
- Gotaas, C., Havelka, P., Jakobsen, H. A., et al. 2007, *Physics of Fluids*, 19, 102106, doi: [10.1063/1.2781603](https://doi.org/10.1063/1.2781603)
- Gunkelmann, N., Kataoka, A., Dullemond, C. P., & Urbassek, H. M. 2017, *A&A*, 599, L4, doi: [10.1051/0004-6361/201630155](https://doi.org/10.1051/0004-6361/201630155)
- Hansen, B. M. S. 2009, *ApJ*, 703, 1131, doi: [10.1088/0004-637X/703/1/1131](https://doi.org/10.1088/0004-637X/703/1/1131)
- Hasegawa, Y., Turner, N. J., Masiero, J., et al. 2016, *ApJL*, 820, L12, doi: [10.3847/2041-8205/820/1/L12](https://doi.org/10.3847/2041-8205/820/1/L12)
- Henke, S., Gail, H.-P., Trieloff, M., Schwarz, W. H., & Kleine, T. 2012a, *A&A*, 537, A45, doi: [10.1051/0004-6361/201117177](https://doi.org/10.1051/0004-6361/201117177)
- . 2012b, *A&A*, 545, A135, doi: [10.1051/0004-6361/201219100](https://doi.org/10.1051/0004-6361/201219100)
- Hewins, R. H., & Radomsky, P. M. 1990, *Meteoritics*, 25, 309, doi: [10.1111/j.1945-5100.1990.tb00715.x](https://doi.org/10.1111/j.1945-5100.1990.tb00715.x)
- Hood, L. L., & Horányi, M. 1991, *Icarus*, 93, 259, doi: [10.1016/0019-1035\(91\)90211-B](https://doi.org/10.1016/0019-1035(91)90211-B)
- Horányi, M., Morfill, G., Goertz, C. K., & Levy, E. H. 1995, *Icarus*, 114, 174, doi: [10.1006/icar.1995.1052](https://doi.org/10.1006/icar.1995.1052)
- Hubbard, A. 2015, *Icarus*, 254, 56, doi: [10.1016/j.icarus.2015.02.030](https://doi.org/10.1016/j.icarus.2015.02.030)
- Iida, A., Nakamoto, T., Susa, H., & Nakagawa, Y. 2001, *Icarus*, 153, 430, doi: [10.1006/icar.2001.6682](https://doi.org/10.1006/icar.2001.6682)
- Jacquet, E. 2014, *Icarus*, 232, 176, doi: [10.1016/j.icarus.2014.01.012](https://doi.org/10.1016/j.icarus.2014.01.012)
- Jacquet, E., & Thompson, C. 2014, *ApJ*, 797, 30, doi: [10.1088/0004-637X/797/1/30](https://doi.org/10.1088/0004-637X/797/1/30)
- Johansen, A., & Okuzumi, S. 2018, *A&A*, 609, A31, doi: [10.1051/0004-6361/201630047](https://doi.org/10.1051/0004-6361/201630047)
- Johnson, B. C., Minton, D. A., Melosh, H. J., & Zuber, M. T. 2015, *Nature*, 517, 339, doi: [10.1038/nature14105](https://doi.org/10.1038/nature14105)
- Josserand, C., & Thoroddsen, S. T. 2016, *Annual Review of Fluid Mechanics*, 48, 365, doi: [10.1146/annurev-fluid-122414-034401](https://doi.org/10.1146/annurev-fluid-122414-034401)
- Kadono, T., & Arakawa, M. 2005, *Icarus*, 173, 295, doi: [10.1016/j.icarus.2004.08.014](https://doi.org/10.1016/j.icarus.2004.08.014)
- Kita, N. T., & Ushikubo, T. 2012, *Meteoritics and Planetary Science*, 47, 1108, doi: [10.1111/j.1945-5100.2011.01264.x](https://doi.org/10.1111/j.1945-5100.2011.01264.x)
- Kokubo, E., & Ida, S. 1998, *Icarus*, 131, 171, doi: [10.1006/icar.1997.5840](https://doi.org/10.1006/icar.1997.5840)
- Krot, A. N., & Rubin, A. E. 1994, *Meteoritics*, 29, 697, doi: [10.1111/j.1945-5100.1994.tb00787.x](https://doi.org/10.1111/j.1945-5100.1994.tb00787.x)
- Kruijer, T. S., Burkhardt, C., Budde, G., & Kleine, T. 2017, *Proceedings of the National Academy of Science*, 114, 6712, doi: [10.1073/pnas.1704461114](https://doi.org/10.1073/pnas.1704461114)

- Leliwa-Kopystynski, J., Taniguchi, T., Kondo, K., & Sawaoka, A. 1984, *Icarus*, 57, 280, doi: [10.1016/0019-1035\(84\)90073-3](https://doi.org/10.1016/0019-1035(84)90073-3)
- Li, H., Kuschel, M., & Sommerfeld, M. 2016, *Experimental Investigation and Modeling of Coalescence and Agglomeration for Spray Drying of Solutions* (Springer), 205–233. http://dx.doi.org/10.1007/978-3-319-32370-1_6
- Libourel, G., & Portail, M. 2018, *Science Advances*, 4, eaar3321, doi: [10.1126/sciadv.aar3321](https://doi.org/10.1126/sciadv.aar3321)
- Liu, B., & Ormel, C. W. 2018, *A&A*, 615, A138, doi: [10.1051/0004-6361/201732307](https://doi.org/10.1051/0004-6361/201732307)
- Lofgren, G., & Russell, W. J. 1986, *GeoCoA*, 50, 1715, doi: [10.1016/0016-7037\(86\)90133-X](https://doi.org/10.1016/0016-7037(86)90133-X)
- Mai, C., Desch, S. J., Boley, A. C., & Weiss, B. P. 2018, *ApJ*, 857, 96, doi: [10.3847/1538-4357/aab711](https://doi.org/10.3847/1538-4357/aab711)
- Matsumoto, Y., Oshino, S., Hasegawa, Y., & Wakita, S. 2017, *ApJ*, 837, 103, doi: [10.3847/1538-4357/aa607d](https://doi.org/10.3847/1538-4357/aa607d)
- Metzler, K. 2018, *Meteoritics & Planetary Science*, 53, 1489, doi: [10.1111/maps.13091](https://doi.org/10.1111/maps.13091)
- Miura, H., & Nakamoto, T. 2005, *Icarus*, 175, 289, doi: [10.1016/j.icarus.2004.11.011](https://doi.org/10.1016/j.icarus.2004.11.011)
- Miura, H., Nakamoto, T., & Doi, M. 2008a, *Icarus*, 197, 269, doi: [10.1016/j.icarus.2008.04.019](https://doi.org/10.1016/j.icarus.2008.04.019)
- Miura, H., Nakamoto, T., & Susa, H. 2002, *Icarus*, 160, 258, doi: [10.1006/icar.2002.6964](https://doi.org/10.1006/icar.2002.6964)
- Miura, H., Tanaka, K. K., Yamamoto, T., et al. 2010a, *ApJ*, 719, 642, doi: [10.1088/0004-637X/719/1/642](https://doi.org/10.1088/0004-637X/719/1/642)
- Miura, H., & Yamamoto, T. 2014, *AJ*, 147, 54, doi: [10.1088/0004-6256/147/3/54](https://doi.org/10.1088/0004-6256/147/3/54)
- Miura, H., Yasuda, S., & Nakamoto, T. 2008b, *Icarus*, 194, 811, doi: [10.1016/j.icarus.2007.11.005](https://doi.org/10.1016/j.icarus.2007.11.005)
- Miura, H., Yokoyama, E., Nagashima, K., Tsukamoto, K., & Srivastava, A. 2010b, *Journal of Applied Physics*, 108, 114912, doi: [10.1063/1.3504655](https://doi.org/10.1063/1.3504655)
- Miyake, K., & Nakagawa, Y. 1993, *Icarus*, 106, 20, doi: [10.1006/icar.1993.1156](https://doi.org/10.1006/icar.1993.1156)
- Morris, M. A., Boley, A. C., Desch, S. J., & Athanassiadou, T. 2012, *ApJ*, 752, 27, doi: [10.1088/0004-637X/752/1/27](https://doi.org/10.1088/0004-637X/752/1/27)
- Morris, M. A., & Desch, S. J. 2010, *ApJ*, 722, 1474, doi: [10.1088/0004-637X/722/2/1474](https://doi.org/10.1088/0004-637X/722/2/1474)
- Mundo, C. H. R., Sommerfeld, M., & Tropea, C. 1995, *International journal of multiphase flow*, 21, 151, doi: [10.1016/0301-9322\(94\)00069-v](https://doi.org/10.1016/0301-9322(94)00069-v)
- Muranushi, T. 2010, *MNRAS*, 401, 2641, doi: [10.1111/j.1365-2966.2009.15848.x](https://doi.org/10.1111/j.1365-2966.2009.15848.x)
- Murase, T., & McBirney, A. R. 1973, *Geological Society of America Bulletin*, 84, 3563, doi: [10.1130/0016-7606\(1973\)84\(3563:POSCIR\)2.0.CO;2](https://doi.org/10.1130/0016-7606(1973)84(3563:POSCIR)2.0.CO;2)
- Nagasawa, M., Tanaka, K. K., Tanaka, H., et al. 2014, *ApJL*, 794, L7, doi: [10.1088/2041-8205/794/1/L7](https://doi.org/10.1088/2041-8205/794/1/L7)
- . 2019, *ApJ*, 871, 110, doi: [10.3847/1538-4357/aaf795](https://doi.org/10.3847/1538-4357/aaf795)
- Nagashima, K., Moriuchi, Y., Tsukamoto, K., Tanaka, K. K., & Kobatake, H. 2008, *Journal of Mineralogical and Petrological Sciences*, 103, 204, doi: [10.2465/jmps.070620c](https://doi.org/10.2465/jmps.070620c)
- Nagashima, K., Tsukamoto, K., Satoh, H., Kobatake, H., & Dold, P. 2006, *Journal of Crystal Growth*, 293, 193, doi: [10.1016/j.jcrysgro.2006.01.064](https://doi.org/10.1016/j.jcrysgro.2006.01.064)
- Nakamoto, T., & Miura, H. 2004, in *Lunar and Planetary Science Conference Abstracts*, Vol. 35, 1847
- Nakamura, T., Noguchi, T., Tanaka, M., et al. 2011, *Science*, 333, 1113, doi: [10.1126/science.1207758](https://doi.org/10.1126/science.1207758)
- Naue, G., & Bärwolff, G. 1992, *Transportprozesse in Fluiden* (Deutscher Verlag für Grundstoffindustrie, Leipzig)
- Nelson, V. E., & Rubin, A. E. 2002, *Meteoritics and Planetary Science*, 37, 1361, doi: [10.1111/j.1945-5100.2002.tb01034.x](https://doi.org/10.1111/j.1945-5100.2002.tb01034.x)
- Okabayashi, S., Yokoyama, T., Nakanishi, N., & Iwamori, H. 2019, *GeoCoA*, 244, 197, doi: [10.1016/j.gca.2018.10.003](https://doi.org/10.1016/j.gca.2018.10.003)
- Okuzumi, S., Momose, M., Sirono, S.-i., Kobayashi, H., & Tanaka, H. 2016, *ApJ*, 821, 82, doi: [10.3847/0004-637X/821/2/82](https://doi.org/10.3847/0004-637X/821/2/82)
- Pape, J., Mezger, K., Bouvier, A.-S., & Baumgartner, L. P. 2019, *GeoCoA*, 244, 416, doi: [10.1016/j.gca.2018.10.017](https://doi.org/10.1016/j.gca.2018.10.017)
- Pinte, C., Dent, W. R. F., Ménard, F., et al. 2016, *ApJ*, 816, 25, doi: [10.3847/0004-637X/816/1/25](https://doi.org/10.3847/0004-637X/816/1/25)
- Pollack, J. B., McKay, C. P., & Christofferson, B. M. 1985, *Icarus*, 64, 471, doi: [10.1016/0019-1035\(85\)90069-7](https://doi.org/10.1016/0019-1035(85)90069-7)
- Qian, J., & Law, C. K. 1997, *Journal of Fluid Mechanics*, 331, 59, doi: [10.1017/s0022112096003722](https://doi.org/10.1017/s0022112096003722)
- Radomsky, P. M., & Hewins, R. H. 1990, *GeoCoA*, 54, 3475, doi: [10.1016/0016-7037\(90\)90299-Z](https://doi.org/10.1016/0016-7037(90)90299-Z)
- Rubin, A. E. 2000, *Earth Science Reviews*, 50, 3, doi: [10.1016/S0012-8252\(99\)00067-7](https://doi.org/10.1016/S0012-8252(99)00067-7)
- . 2010, *GeoCoA*, 74, 4807, doi: [10.1016/j.gca.2010.05.018](https://doi.org/10.1016/j.gca.2010.05.018)
- Rubin, A. E., & Grossman, J. N. 1987, *Meteoritics*, 22, 237, doi: [10.1111/j.1945-5100.1987.tb00622.x](https://doi.org/10.1111/j.1945-5100.1987.tb00622.x)
- Sanders, I. S., & Scott, E. R. D. 2012, *Meteoritics and Planetary Science*, 47, 2170, doi: [10.1111/maps.12002](https://doi.org/10.1111/maps.12002)
- Scott, E. R. D. 2007, *Annual Review of Earth and Planetary Sciences*, 35, 577, doi: [10.1146/annurev.earth.35.031306.140100](https://doi.org/10.1146/annurev.earth.35.031306.140100)
- Seto, Y., Suzuki, K., Shoda, N., & Ichimura, S. 2017, in *The Eighth Symposium on Polar Science*
- Simon, J. B., Armitage, P. J., Li, R., & Youdin, A. N. 2016, *ApJ*, 822, 55, doi: [10.3847/0004-637X/822/1/55](https://doi.org/10.3847/0004-637X/822/1/55)
- Simon, J. I., Cuzzi, J. N., McCain, K. A., et al. 2018, *Earth and Planetary Science Letters*, 494, 69, doi: [10.1016/j.epsl.2018.04.021](https://doi.org/10.1016/j.epsl.2018.04.021)
- Sommerfeld, M., & Kuschel, M. 2016, *Experiments in Fluids*, 57, 187, doi: [10.1007/s00348-016-2249-y](https://doi.org/10.1007/s00348-016-2249-y)
- Srivastava, A., Inatomi, Y., Tsukamoto, K., Maki, T., & Miura, H. 2010, *Journal of Applied Physics*, 107, 114907, doi: [10.1063/1.3406149](https://doi.org/10.1063/1.3406149)

- Stewart, S. T., & Leinhardt, Z. M. 2009, *ApJL*, 691, L133, doi: [10.1088/0004-637X/691/2/L133](https://doi.org/10.1088/0004-637X/691/2/L133)
- Susa, H., & Nakamoto, T. 2002, *ApJ*, 564, L57, doi: [10.1086/338789](https://doi.org/10.1086/338789)
- Tachibana, S., & Huss, G. R. 2005, *GeoCoA*, 69, 3075, doi: [10.1016/j.gca.2004.06.025](https://doi.org/10.1016/j.gca.2004.06.025)
- Tammann, G., & Hesse, W. 1926, *Zeitschrift für anorganische und allgemeine Chemie*, 156, 245, doi: [10.1002/zaac.19261560121](https://doi.org/10.1002/zaac.19261560121)
- Tang, C., Zhang, P., & Law, C. K. 2012, *Physics of Fluids*, 24, 022101, doi: [10.1063/1.3679165](https://doi.org/10.1063/1.3679165)
- Toomre, A. 1964, *ApJ*, 139, 1217, doi: [10.1086/147861](https://doi.org/10.1086/147861)
- Tsuchiyama, A., Shigeyoshi, R., Kawabata, T., et al. 2003, in *Lunar and Planetary Science Conference Abstracts*, Vol. 34, 1271
- Tsukamoto, K., Satoh, H., Takamura, Y., & Kuribayashi, K. 1999, *Antarctic Meteorites*, 24, 179
- Ueda, T., Murakami, Y., Ishitsu, N., et al. 2001, *Earth, Planets, and Space*, 53, 927, doi: [10.1186/bf03351689](https://doi.org/10.1186/bf03351689)
- Uesugi, M., Akaki, T., Sekiya, M., & Nakamura, T. 2005, *Meteoritics and Planetary Science*, 40, 1103, doi: [10.1111/j.1945-5100.2005.tb00175.x](https://doi.org/10.1111/j.1945-5100.2005.tb00175.x)
- Uesugi, M., Sekiya, M., & Nakamura, T. 2008, *Meteoritics and Planetary Science*, 43, 717, doi: [10.1111/j.1945-5100.2008.tb00680.x](https://doi.org/10.1111/j.1945-5100.2008.tb00680.x)
- Villeneuve, J., Libourel, G., & Soulié, C. 2015, *GeoCoA*, 160, 277, doi: [10.1016/j.gca.2015.03.033](https://doi.org/10.1016/j.gca.2015.03.033)
- Vogel, H. 1921, *Physikalische Zeitschrift*, 22, 645
- Wakita, S., Matsumoto, Y., Oshino, S., & Hasegawa, Y. 2017, *ApJ*, 834, 125, doi: [10.3847/1538-4357/834/2/125](https://doi.org/10.3847/1538-4357/834/2/125)
- Walsh, K. J., & Levison, H. F. 2016, *AJ*, 152, 68, doi: [10.3847/0004-6256/152/3/68](https://doi.org/10.3847/0004-6256/152/3/68)
- Walzel, P. 1980, *Chemie Ingenieur Technik*, 52, 338, doi: [10.1002/cite.330520412](https://doi.org/10.1002/cite.330520412)
- Wasson, J. T. 1993, *Meteoritics*, 28, 14, doi: [10.1111/j.1945-5100.1993.tb00244.x](https://doi.org/10.1111/j.1945-5100.1993.tb00244.x)
- . 2012, *Meteoritics and Planetary Science Supplement*, 75, 5083
- Wasson, J. T., & Kallemeyn, G. W. 1988, *Philosophical Transactions of the Royal Society of London Series A*, 325, 535, doi: [10.1098/rsta.1988.0066](https://doi.org/10.1098/rsta.1988.0066)
- Wasson, J. T., Krot, A. N., Lee, M. S., & Rubin, A. E. 1995, *GeoCoA*, 59, 1847, doi: [10.1016/0016-7037\(95\)00087-G](https://doi.org/10.1016/0016-7037(95)00087-G)
- Wasson, J. T., & Rubin, A. E. 2003, *GeoCoA*, 67, 2239, doi: [10.1016/S0016-7037\(03\)00023-1](https://doi.org/10.1016/S0016-7037(03)00023-1)
- Weidenschilling, S. J. 1977, *MNRAS*, 180, 57, doi: [10.1093/mnras/180.1.57](https://doi.org/10.1093/mnras/180.1.57)
- Weidenschilling, S. J., Marzari, F., & Hood, L. L. 1998, *Science*, 279, 681, doi: [10.1126/science.279.5351.681](https://doi.org/10.1126/science.279.5351.681)
- Willis, K., & Orme, M. 2003, *Experiments in Fluids*, 34, 28, doi: [10.1007/s00348-002-0526-4](https://doi.org/10.1007/s00348-002-0526-4)
- Xiang, C., Carballido, A., Hanna, R. D., Matthews, L. S., & Hyde, T. W. 2019, *Icarus*, 321, 99, doi: [10.1016/j.icarus.2018.10.014](https://doi.org/10.1016/j.icarus.2018.10.014)
- Yang, C.-C., Johansen, A., & Carrera, D. 2017, *A&A*, 606, A80, doi: [10.1051/0004-6361/201630106](https://doi.org/10.1051/0004-6361/201630106)
- Yasuda, S., Miura, H., & Nakamoto, T. 2009, *Icarus*, 204, 303, doi: [10.1016/j.icarus.2009.06.014](https://doi.org/10.1016/j.icarus.2009.06.014)
- Youdin, A. N., & Lithwick, Y. 2007, *Icarus*, 192, 588, doi: [10.1016/j.icarus.2007.07.012](https://doi.org/10.1016/j.icarus.2007.07.012)
- Zanda, B. 2004, *Earth and Planetary Science Letters*, 224, 1, doi: [10.1016/j.epsl.2004.05.005](https://doi.org/10.1016/j.epsl.2004.05.005)